Thesis of Doctoral Degree

Raman Spectroscopy for Real Time Monitoring of Cancer in Live Mouse Models

Department of Bioscience, Graduate School of Science and Technology

Kwansei Gakuin University

Akinori Taketani

February 28, 2018

Abstract

The purpose of these studies was to develop Raman spectroscopic techniques to support *in situ* cancer diagnosis during endoscopic observation. Reliable diagnostic techniques are essential for cancer diagnosis, which may reduce invasiveness and provide objective data, thus improving the accuracy of endoscopic diagnosis.

The aim of the first study was to evaluate the capability of a miniaturized Raman endoscope (mRE) system to monitor the advancement in colorectal tumors in a mouse model. The endoscope was narrow enough to observe the internal portion of the mouse colon in a semi-noninvasive method, following anesthesia treatment. The mRE system allowed the visualization and Raman spectral measurement of any targeted point within the colorectal tumor in the model animal under anesthesia, with no damage to the tissue (i.e., noninvasive method). Continuous monitoring of the same tumor allowed observation of the alteration in its molecular composition and size, as well as the tumor advancement. The tumor lesion was distinguished from the normal tissues of the control mouse at an accuracy of 86.8%. The Raman spectra obtained from the live mouse colon revealed molecular changes in lipid and protein profiles. As the next step, it would be necessary to evaluate the effectiveness of the mRE system.

In the second study, the effects of anticancer drugs were studied using the mRE system in the mouse model. Three anticancer drugs, 5-fluorouracil (5-FU), cisplatin (CDDP), and docetaxel were employed for this purpose. This study demonstrated that *in situ* Raman analysis is highly sensitive in detecting the effects of anticancer drugs. On the other hand, a noninvasive technique was developed to collect images, as one of the standards for diagnosis.

The third study investigated the site dependency in cancer tissue using unstained

autofluorescence hyperspectral imaging (AF-HSI) and Raman spectroscopy. AF-HSI images reflected the distribution of intact fluorescence materials such as nicotinamide adenine dinucleotide (NADH), flavin adenine dinucleotide (FAD), and collagen in the subcutaneous tumor in a live mouse model. Raman spectroscopy showed the difference in blood flow between the active and non-active areas with NADH imaging. AF-HSI image *in situ* and Raman spectroscopy revealed the distribution of collagen type I. AF-HSI images gathered information that was inaccessible using tissue sections. The measurement methods using the mouse model, Raman spectroscopy, and autofluorescence imaging were important tools to study cancer progression and anticancer drug treatment.

<<CONTENTS>>

General Introduction

Colorectal cancer is the most common cause of cancer deaths in women and the third most common cause of cancer deaths in men in Japan[1]. In Japan, colon examination is conducted through screening tests for the early detection and diagnosis of colorectal cancer. Patients are diagnosed with other methods upon detection of blood in the stool. A blood test is generally the second preferred method for the detection of cancer markers and may be the most convenient method with less impact on the patient's health[2]. Precision examination is performed after the blood test. Endoscope test and histopathology using tissue biopsy are standard methods that directly analyze lesions in the colon[3]. The reliability of endoscopic observations largely depends on the knowledge and skill of the clinicians. J. C. Rijn reported a global miss rate of 21% in the detection of colorectal polyps with endoscopy[4]. This report is expected to improve the accuracy of the endoscopic diagnosis. Some additional techniques have been developed to allow visualization of the fine texture of the tissue surface during endoscopy, such as spraying indigo carmine dye, narrow band imaging observation, and auto-fluorescence imaging[5-7]. Cancer diagnosis based on visual observation fully relies on the pattern recognition ability or "esthetic eyes'" of clinicians. In addition to the direct observation of colorectal cancer with an endoscope, a few methods that allow cancer detection in a completely noninvasive manner include X-ray computed tomography (X-CT), magnetic resonance imaging (MRI), and positron emission tomography (PET), which allow visualization of the tumor shape[8-10]. Although the accuracy of diagnosis by X-CT, MRI, and PET is increasing every year, the results may not be convincing enough for the clinicians. As X-ray CT poses the risk of the exposure to radiation, it is not easily recommended to patients from time to time. MRI may pose difficulty in the clear observation of the colon structure,

as the colon moves during peristaltic exercise and the measurements may take a long time. Although PET is a powerful technology to detect metastasized cancer, very few hospitals have this facility. These techniques (X-CT, MRI, PET, and endoscopy) rely on the morphological observations such as the shape and size of the suspicious lesion, and clinicians often require additional direct observation of the tissue to make confirmatory diagnosis. Histopathology with tissue biopsy is a gold standard for the definite diagnosis of cancer. However, it is highly invasive and requires a long time for sample preparation before microscopic observation. The number of pathologists in 2017 is 2,405, and the number of hospitals is 8,439. It is concerned that the load of pathologists increases rapidly as the number of biopsy required increases. Hence, reliable diagnostic techniques that reduce invasiveness and provide objective data are desirable to improve the accuracy of endoscopy-based cancer diagnosis.

In recent years, Raman spectroscopy has attracted the attention of researchers as a technique for cancer diagnosis. It is one of the measurement techniques that provide subjective data of biological samples with low invasiveness. In 1928, C. V. Raman discovered scattered light exhibiting different frequencies upon irradiation of carbon tetrachloride (CCl_4) with monochromatic light, for which he was awarded the Nobel Prize in 1930. This phenomenon, termed as the Raman effect, after his name[11,12], is attributed to energy transition in a molecule between the ground state and the excited vibrational state. As the vibrational level is unique to the molecule, vibrational spectroscopy is able to determine and identify molecules present in any sample. The applications of Raman spectroscopy were limited until the development of the first laser in 1960. Many researchers have used Raman spectroscopy to study biological samples, owing to its low invasiveness[13]. Ozaki et al. obtained the Raman spectra of proteins from the eye lens using

argon ion visible excitation laser (488 nm)[14]. However, almost all biomaterials emit strong fluorescence and are weak substrates for laser illumination[15]. Fluorescence may pose a problem while using Raman spectroscopy for biological samples. In 1980s, Fourier transform (FT) Raman spectroscopy that employs an oscillation line of Nd-YaG laser at 1064 nm for light excitation was developed to eliminate fluorescence noise[15,16]. Raman spectra of many biological samples were successfully obtained using FT Raman spectroscopy. However, the detection sensitivity was low and the time to measure FT Raman spectrum was considerable. In the 1990s, a different type of near-infrared (NIR) excitation Raman spectrometer equipped with a sensitive and commercial charge-coupled device (CCD) detector, a high throughput dispersion spectrometer, and an NIR diode laser that emitted light from 700 to 860 nm wavelength became popular. This instrument allowed the measurement of Raman spectrum in a shorter time than that with the FT Raman instrument. Coupling it with an optical fiber was easy, as NIR light exhibits high throughput in normal glass fiber for biomedical Raman spectroscopy[17,18].

In comparison with other vibrational spectroscopy techniques, NIR excitation Raman spectroscopy offers some advantages. Fourier transformed infrared (FT-IR) absorbance spectroscopy, a technique related to Raman spectroscopy, is one of the vibrational spectroscopy methods[19] used for the analysis of organic materials. However, FT-IR spectroscopy may not be useful for biomedical study. As water has high absorption in infrared and NIR regions, it is difficult to measure water-based samples such as biological samples with FT-IR spectroscopy. Materials with covalent bonds exhibit vibrational energy. IR light has very low penetration efficiency for most of the optical materials. Currently, very few materials are available for optical fiber IR light. In contrast, visible and NIR light (~1200 nm) are used for the measurement of Raman spectrum. Glass

and water have no absorption in these regions. Moreover, the Raman band of water does not overlap with the finger print region (~1800 cm^{-1}) of usual organic materials. All these features deem Raman spectroscopy suitable for bioanalysis.

Raman spectra of biological materials comprise complex bands, owing to the overlapping peaks arising from various chemical materials[20]. Chemometrics, a mathematical technique based on statics, is applied to analyze complex data and extract useful information from a series of datasets for easy understanding. Chemometrics allows visualization and easy understanding of the change in the data group without arbitrariness, thereby serving as an important tool for the analysis of Raman spectra of biological samples.

Many researchers have reported *in situ* analysis of cancers by Raman spectroscopy and fiber optic Raman probes. Raman spectroscopy was applied for the first time to explore the implications of early detection of neoplastic lesions in the human stomach during clinical gastroscopic observation. Bergholt et al. developed a 1.8-mm diameter Raman probe for its use in the human stomach[21] and suggested that cancerous tissues could be identified in the stomach and esophagus at an accuracy of 89.3% and 94.7%, respectively, using Raman spectroscopy and partial least squares-discriminant analysis (PLS-DA) as one of the chemometrics[22]. Furthermore, Haka et al. suggested the application of Raman endoscopy for human breast cancer diagnosis (*ex vivo* study)[23].

The purpose of this study was to develop Raman spectroscopic techniques for supporting *in situ* cancer diagnosis with endoscopic observation. This study may provide objective data to clinicians to improve the accuracy of endoscopic diagnosis. In this direction, fundamental research on colorectal cancer tissues using Raman spectroscopy is desirable. Many researchers have developed techniques to discriminate between benign

and malignant tumor. Clinicians may not rely on Raman spectroscopy data for making confirmatory diagnosis, as Raman spectroscopy shows no morphological information but may provide detailed information of molecular composition changes. Therefore, it is necessary to accumulate sufficient amount of basic data and research results to prove reliable diagnosis with Raman spectroscopy in the absence of morphological information. To the best of my knowledge, no technique allows the direct observation of the advancement in cancer. M. V. Schulmerich et al. reported *in vivo* measurement of murine bones under anesthesia using Raman spectroscopy[24]. The present study was encouraged based on the results of previous studies for monitoring the tumor (colorectal tumor) in a single living mouse model to provide sufficient reliable data.

The use of a mouse model offers several advantages. It is possible to monitor the advancement of tumor from early stages and during the chemotherapy treatment process using a mouse model. Moreover, the individual discordance is eliminated, as the mice are isogenic. The azoxymethane–dextran sodium sulfate (AOM–DSS) colon cancer mouse model was used in the present study, as the tumor advances very rapidly in this model, and a month is enough for the sample preparation[25]. The tumor often advances into adenocarcinoma in this model[26], which was used herein to monitor the advancement of tumors, using Raman spectroscopy. The problem in using a mouse model was its small size. The normal endoscope with the Raman probe used for human studies was too large for the mouse model. Hattori et al. and Komachi et al. developed a miniaturized Raman endoscopic (mRE) system for mouse studies[27-29]. The diameter of the endoscope head was 2.5 mm and included a channel with a 1.2-mm diameter. A ball lens-installed hollow optical fiber Raman probe (BHRP) with a 0.64-mm diameter was attached on to the probe head[30–32]. This system was small enough to measure the mouse colon tumor under

anesthesia treatment, while BHRP allowed noninvasive measurement of tissues. The first study involved the use of established techniques for *in situ* noninvasive observation of the same tumor to monitor the advancement of cancer in a live mouse model using an mRE system with BHRP and development of procedures for the efficient analysis of the Raman spectra with chemometrics. In the next step, the efficiency of this instrument was evaluated. In the second study, the effects of anticancer drugs were studied using an mRE system in the mouse model. Anticancer drug treatment is one of the standard treatments for colorectal cancer. Monitoring the effect of anticancer drugs by Raman spectroscopy has been conducted in cultured cells[33]. Skolekova et al. reported the effects of anticancer agents on cancer cells[34]. Ock et al. reported real-time monitoring of anticancer drug effects on cancer cells using surface-enhanced Raman spectroscopy[35]. These studies strongly suggest that Raman spectroscopy may be useful for monitoring the effects of anticancer drugs at the cellular level. The molecular biological study of cultured cancer cells may provide information on the anticancer effects of drugs. However, this information may be insufficient to understand cancer tissue, owing to the complexity of cancer tissues as compared with cells[36]. The mRE system and mouse model allowed direct monitoring of tumors.

Under clinical settings, cancer diagnosis is based on imaging techniques such as histopathology and endoscopic diagnosis. The Raman image system comprises a microscope Raman spectrometer and confocal imaging system on a computed micro-stage. The sample for observation may be inserted into the sampling stage of the microscope. It is necessary to process the sample and it may be difficult to evaluate live tissues. Autofluorescence imaging has been used to study colorectal cancer. Aubin et al. suggested that nicotinamide adenine dinucleotide (NADH) and flavin exhibit

autofluorescence in viable cells[37]. Barenbiom et al. reported that elastin and collagen present extensively in the extracellular matrix and emit autofluorescence[38]. The measurement of NADH in viable cells and extracellular matrix may provide structural information of the tumor tissue, as tumor tissue contains complex structures such as cancer stem cells and extracellular matrix. The site dependency of viable cells and extracellular matrix was studied in live tumors by comparing the autofluorescence image with Raman spectra to study the complex structure of tumor tissues in third chapter.

The first and second chapters have already been published in journals[39,40].

References

1. Cancer statistics in Japan, *FPCR National Cancer Center*, 2015
2. P. Hewitson, P. Glasziou, E. Watson, B. Towler and L. Irwig, *Am. J. Gastroenterol.,* 2008, **10**, 1572
3. K. W. Kinzler and B. Vogelstein, *Cell*, 1996, **87**, 159-170
4. J.C. Rijn, J. B. Reitsma, J. Stoker, P. M. Bossuyt, S. J. Deventer and E. Dekker, *Am. J. Gastroenterol.*, 2006, **10**, 343-350
5. S. Kudo, H. Kashida, T. Tamura, E. Kogure, Y. Imai, H. Yamano and A. R. Hart, *World J. Surg*., 2000, **24**, 1081-1090
6. N. Uedo, H. Iishi, M. Tatsuta, T. Yamada, H. Ogiyama, K. Imanaka, N. Sugimoto, K. Higashino, R. Ishihara, H. Narahara and S. Ishiguro, *Gastrointest. Endosc.*, 2005, **62**, 521-528
7. H. M. Chiu, C. Y. Chang, C. C. Chen, Y. C. Lee, M. S. Wu, J. T. Lin,C. T. Shun and H. P. Wang, *Gut.*, 2007, **56,** 373–379
8. O. A. Ogunbiyi, F. L. Flanagan, F. Dehdashti, B. A. Siegel, D. D. Trask, E. H. Birnbaum, J. W. Fleshman, T. E. Read, G. W. Philpott and I. J. Kodner, *Ann. Surg. Oncol.*, 1997, **4**, 613-620
9. T. Ichikawa, S. M. Erturk, U. Motosugi, H. Sou, H. Iino, T. Araki and H. Fujii, *AJR*, 2006, **187**, 181-184
10. D. Dominique, *J. Nucl. Med.,* 1999, **40**, 591-603
11. C. V. Raman, K. S. Krishnan, *Nature*, 1928, **121** , 501-502
12. C. V. Raman, K. S. Krishnan, *Nature*, 1928, **121**, 711-711
13. E. B. Hanlon, R. Manoharan, T. W. Koo, K. E. Shafer, J. T. Motz, M. Fitzmaurice, J. R. Kramer, I. Itzkan, R. R. Dasari and M. S. Feld, *Phys. Med. Biol.* 2000, **45**, R1-R59

14. A. Mizuno, Y. Ozaki, K. Itoh, S. Matsushima and K. Iriyama, *Biochem. Biophys. Res. Commun.* 1984, **119**, 989-994

15. Y. Ozaki, A. mizuno, H. Sato, K. Kawauchi, *Appl. Spectrosc.* 1992, **46**, 533-536

16. B. Venkatesh, S. Ramasamy, M. Mylrajan, R. Asokan, P. T. Manoharan and J. M. Rifkind, *Spectrochim. Acta. A.,* 1999, **55**, 1691-1697

17. C. J. Frank and R. L. McCreery, *Anal. Chem.*, 1995, **67**, 777

18. J. F. Brennan III, Y. Wang, R. R. Dasari amd S. Feld, *Appl. Spectrosc.* 1997, **51**, 201

19. Z. Movasaghi, S. Rehman and I. ur Rehman, *App. Spectrosc. Rev.*, 2008, **43**, 134–179

20. I. Notingher, C. Green, C. Dyer, E. Perkins, N. Hopkins, C. Lindsay and L. L. Hench, *J. R. Soc. Interface,* 2004, **1**, 79–90

21. M. S. Bergholt, W. Zheng, K. Lin, K. Y. Ho, M. Teh, K. G. Yeoh, J. B. Y. So and Z. Huang, *Analyst,* 2010, **135**, 3162–3168

22. M. S. Bergholt, W. Zheng, K. Lin, K. Y. Ho, M. Teh, K. G. Yeoh, J. B. Y. So and Z. Huang, *J. Biomed. Opt.*, 2011, **16**, 037003

23. A. S. Haka, Z. Volynskaya, J. A. Gardecki, J. Nazemi, R. Shenk, N. Wang, R. R. Dasari, M. Fitzmaurice and M. S. Feld, *J. Biomed. Opt*., 2009, **14**, 054023

24. M. V. Schulmericha, J. H. Colea, J. M. Kreiderb, F. E. Whitea, K. A. Dooleya, S. A. Goldsteinb and M. D. Morrisa, *Appl. Spectrosc*., 2009, **63**, 286–295

25. D. W. Rosenberg, C. Giardina and T. Tanaka, *Carcinogenesi*s, 2009, **30**, 183–196

26. C. Becker, M. C. Fantini, S. Wirtz, A. Nikolaev, R. Kiesslich, H. A. Lehr, P. R. Galle and M. F. Neurath, *Gut*, 2005, **54**, 950–954

27. Y. Hattori, Y. komachi, T. Asakura, T. Shimosegawa, G. Kanai, H. Tashiro and H. Sato, *App. Spec.,* 2007, **6**, 579-584

28. Y. Komachi, T. Katagiri, H. Sato and H. Tashiro, *Appl. Opt*., 2009, **48**, 1683-1696

29. Y. Komachi, H. Sato, K. Aizawa and H. Tashiro, *Appl. Opt*., 2005, **44**, 4722-4732

30. T. Katagiri, Y. S. Yamamoto, Y. Ozaki, Y. Matsuura and H. Sato, *Appl. Spectrosc*., 2009, **63**, 103-107

31. Y. S. Yamamoto, Y. Oshima, H. Shinzawa, T. Katagiri, Y. Matsuura, Y. Ozaki and H. Sato, *Anal. Chim.*, 2008, **619**, 8-13

32. B. B. Andriana, Y. Oshima, S. Takanezawa, T. W. Tay, C. L. R. Soeratman, M. S. Alam, H. Mitsuoka, X. B. Zhu, T. Suzuki, Y. S. Yamamoto, N. Tsunekawa, Y. Kanai, M. Kurohmaru and H. Sato, BiOS-SPIE, San Jose, California, USA, 2009, 7167-33.

33. R. J. Swain and M. M. Stevens, *Biochem. Soc. Trans.,* 2007, **35**, 549

34. S. Skolekova, M. Matuskova, M. Bohac, L. Toro, L. Demkova and J. Gursky, *Cell Commun. Signaling,* 2016, **14**, 4

35. K. Ock, W. I. Jeon, E. O. Ganbold, M. Kim, J. Park, J. H. Seo, K. Cho, S. W. Joo and S. Y. Lee, *Anal. Chem*., 2012, **84**, 2172-2178

36. D. Hanahan and R. A. Weinberg, *Cell*, 2000, **100**, 57-70

37. J. E. Aubin, J. Histochem. *Cytochem*., 1979, **27**, 36-43

38. G. M. Barenboim, A. N. Domanskii, K. K. Turoverov, *New York*, 1969, **6**

39. A. Taketani, R. Hariyani, M. Ishigaki, B. B. Andriana and H. Sato, *Analyst*, 2013, **138**, 4183-4190

40. A. Taketani, B. B. Andriana, H. Matsuyoshi and H. Sato, *Analyst*, 2017, **142**, 3680–3688

Chapter I : Raman Endoscopy for the *in situ* investigation of advancing colorectal tumors in live model mice

I - 1. Abstract

The aim of the present study is to evaluate the capability of a miniaturized Raman endoscope (mRE) system to monitor the advancement of colorectal tumors in model mice as a method that is noninvasive to the tumor itself. Nevertheless, the endoscope is narrow enough to observe the inside of the mouse colon in such a way that is semi-noninvasive to the animal. However, the mRE system allowed the visualization and Raman spectral measurement of any targeted point within the colorectal tumor in model mice under anesthesia, without damaging the tissue (i.e., noninvasively). Continuous monitoring of the same tumor allowed the observation of alterations in its molecular composition and size, along with its advancement. The tumor lesion was discriminated from normal tissues of the control mouse with an accuracy of 86.8%. I succeeded in visualizing and performing Raman spectral observations on a shrinking polyp type tumor. The Raman analysis suggested that it was not cured but supposedly transformed to another tumor type.

I - 2. Introduction

Colorectal cancer is the third most cancer death in men and first most cancer death in women in Japan[1]. Colorectal cancer is generated by mutations in tumor-suppressor genes and oncogenes activated in the colon epithelium. After further mutations in tumor-suppressor genes such as p53, matrix metalloproteinase is expressed in the tumor cells, leading to the destruction of the basal lamina consisting of collagen IV, and then the tumor acquires the ability to metastasize[2,3]. Early stage tumors in the colorectal epithelium are generally benign and usually in the form of an adenoma. However, these tumors can metastasize, and therefore, be classified as adenocarcinoma. Determining whether a tumor is malignant or benign is difficult based on its visual appearance[4,5].

Raman spectroscopy had been applied to explore the implications of early detection of neoplastic lesions in the human stomach during clinical gastroscopy, and excitation laser was introduced a 1.8 mm Raman endoscopic probe for the *in situ* measurement[6]. Bergholt et al., reported that cancerous tissues could be identified inside the stomach and esophagus with an accuracy of 89.3% and 94.7%, respectively[6,7]. Meanwhile, Raman endoscopy can be suggested for human breast cancer diagnosis (*ex vivo study*)[8]. Their results showed a sensitivity of 83% and a specificity of 93% for the evaluation of freshly excised surgical specimens[8]. In the case of colorectal cancer diagnosis, Zheng et al. reported about the Raman analysis of single live epithelial cells, in which the method showed about 86.3% sensitivity and 86.3% specificity[9].

The purpose of the present study is to demonstrate that the molecular changes of a tumor lesion can be studied over a long period in a live mouse by using the miniaturized Raman endoscope (mRE) system. The use of a mouse model makes it possible to monitor the advancement of the tumor from the very early stage through the treatment process

during chemotherapy. Moreover, it can eliminate individual discordance. In generating the tumor model, the same tumor type is usually produced because the mouse is isogenic; moreover, the initiator and the promoter of carcinogenesis are identical to all the mice. It is impossible to do a similar observation in human subjects. Nevertheless, the problem in using a mouse model is its size. The normal endoscope with a Raman probe used for human studies is too large for the mouse model. Hence, we developed the present mRE system for mouse studies[10-12]. The diameter of the endoscope head is 2.5 mm, including a channel with 1.2 mm diameter. A ball lens-installed hollow optical fiber Raman probe (BHRP) with 0.64 mm diameter is inserted into the channel[13–15]. Raman spectroscopy allows us to obtain information about molecular concentrations and the structural composition of tumor tissues *in situ* in a totally noninvasive manner. The long-term aim of this study is to develop a technique for analyzing the characteristic molecular compositions of adenomas and adenocarcinomas, and for monitoring the effect of anticancer drugs *in situ.* To reach this aim, the present study focuses on collecting preliminary knowledge and examining the performance of the system. We have developed a method for monitoring the molecular changes in an axillary tumor in a living rat by injecting BHRP into the tumor via an injection needle[15]. The early detection of the cancer is not the major purpose at this time.

The azoxymethane–dextran sodium sulfate (AOM–DSS) colon cancer model mice were used in the present study because the tumor advances very rapidly in this model and only 1 month is needed for sample preparation[16]. AOM-DSS model has been found to be more potent and stable in solution than 1,2-dimethylhydrazine models[17]. Moreover, the tumor often advances into adenocarcinoma in this model[18]. However, no concrete knowledge is available about the advancement of these tumors. Therefore, monitoring the

same tumor (colorectal tumor) in a single mouse is necessary for a reliable analysis. In the present study, performing Raman measurement under the guide of visual observation in individual live mice and analyzing the molecular alterations dependent on the advancement of the tumor were successfully carried out.

I - 3. Material and Methods

1. Preparation of AOM–DSS colorectal cancer model mice

BALB/cCrSlc mice were purchased from SLC (Shizuoka, Japan). The azoxymethane (AOM) and dextran sodium sulfate (DSS) were purchased from Sigma-Aldrich Chemical Co. (St. Louis, MO, USA). The saline (Otsuka Pharmaceutical Co., Ltd., Tokushima, Japan) solution of AOM was administrated by intraperitoneal injection (7.4 mg kg^{-1}) once to each 8 week old mouse[17]. The mice were then given DSS in drinking water (30 mg ml^{-1}). DSS administration had a duration of 1 week and was repeated twice with a 2 week interval[16]. A tumor was observed in all mice (16 heads) at 15 weeks after AOM administration. Four of 16 heads mice, which have developed tumor lesions, possessed good recognizable tumor performance for Raman measurement and were used for further studies. Several control mice were kept under the same conditions as the model mice. Measurements of 3 model mice (A–C) and 1 control mouse (N) were carried out at 15, 17, and 19 weeks of age, and the remaining model mouse (D) was assessed at 16 and 18 weeks. Carcinogenesis of these colorectal tumors was confirmed by histopathological study in Biopathology Institute Co., Ltd(Oita, Japan).

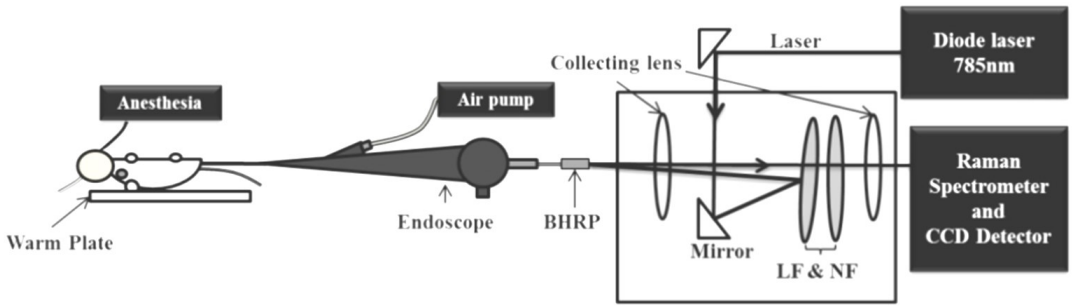

Fig.1-1 The structure of the miniaturized Raman endoscopic system with schematic drawing of the experimental setup.

2. Raman measurements

The Raman system was equipped with a miniaturized endoscope and a ball lens-installed hollow optical fiber Raman probe (BHRP)[13-15]. The endoscope was made by Machida Endoscope Co. Ltd. (Japan). The homemade BHRP consisted of a sapphire ball lens of 500 mm diameter (Edmund Optics, USA) and a hollow optical fiber of 420 mm outer diameter (Doko Engineering LLC, Japan)[9-12]. Combining miniturized endoscope and BHRP made mRE system. A diode laser emitting at 785 nm (Toptica Photonics, Germany) was used for excitation during the Raman measurements. A single polychromatic Raman spectrometer (F4.2, focal length 320 mm, 750 nm blazed 600 l mm^{-1} grating; Photon Design Co. Ltd., Japan) and a charge coupled device detector (DU420-BRDD; Andor Technology Co. Ltd., Northern Ireland) were used to record the Raman spectra. The BHRP was coupled to the spectrometer through a long-pass filter (LF; Semrock, USA), a notch filter (NF; Kaiser Optical System, USA), and 2 lenses to focus the laser and Raman scattered light into the hollow optical fiber and the slit (100 mm width). Fig. 1-1 describes this mini-endoscope and Raman system. Spectra for a 60 second exposure of the sample to a 60 mW excitation light were acquired.

3. Procedure for endoscopic observation

Mice were anesthetized with an inhalation anesthesia apparatus (SurgiVet, USA) and kept on a warming plate to maintain the body temperature at about 37 ℃. The mice were then positioned on a specialized circuit board that can control heating[19]. The concentration of isoflurane (Mylan, Tokyo, Japan) was 1.0–2.5%. Isoflurane has a lower concentration than that is recommended by Piramal Healthcare Ltd., London, UK with the volume-to-volume (v/v) of 3–5%[19]. The endoscope was inserted from the anus, and then the lumen was pressurized with air via the channel to keep the field of view. Feces that remained in the colon were removed by washing off the colon with saline. The BHRP was inserted into the endoscope's channel to measure the Raman spectra (Fig. 1-1). The distance of the tumor from the anus was recorded through repeated measurements. The method worked well, and no other markers were necessary for recognizing the same tumor in each mouse during this experiment. This study was approved by the ethics committee of Kwansei Gakuin University.

4. Histology study

Particularly in histology studies, whole specimens are immediately fixed with 4% paraformaldehyde at 4 ℃, dehydrated through a graded series of ethanol (70%, 80%, 90%, 95%, and 100%), continued immersing in histo-clear, and embedded in paraffin[20]. The sections were 5 μm thick and stained with hematoxylin–eosin (H/E). The degree of morphological alteration in the tissue sections was graded by experienced pathologists who were blind to spectroscopic data.

5. Data analysis

First, a background spectrum due to the Raman probe was subtracted from the recorded spectra, and the measured spectra were later background-corrected. The 5th polynomial line fit to the spectrum was subtracted from the spectra. Spectral areas having a negative value were extracted. The extracted areas were subjected to a 5th polynomial fitting and another subtraction. The same procedure was repeated 5 times to obtain the background-corrected spectra. Then, the spectral intensities were standardized with a phenylalanine band at 1003 cm^{-1}, which was adequately sharp to determine its accurate intensity. These collection procedures are necessary for the further analysis[8]. A chemometrics software program (Unscrambler; CAMO, USA) was used for principal component analysis (PCA), partial least square regression (PLSR) analysis, and linear discriminant analysis (LDA)[21,22]. PCA is able to obtain the maximum variance from complex data as the principal component (PC) and find the correlation of these data. PLSR, similar method to PCA, find the linear differences from complex data as the factor. LDA is a classification method of searching for a linear combination of the variables that best separates two classes. The minimum level of smoothing (11 points) was carried out with the Savitzky–Golay method to show the bands clearer to the spectra shown in Fig. 1-2. However, the spectra without smoothing were used for the further spectral analysis to minimize the artificial effect.

I - 4. Results

1. Raman measurements of colorectal tumors in model mice

Mice that have too large tumors in the rectum were excluded from the study due

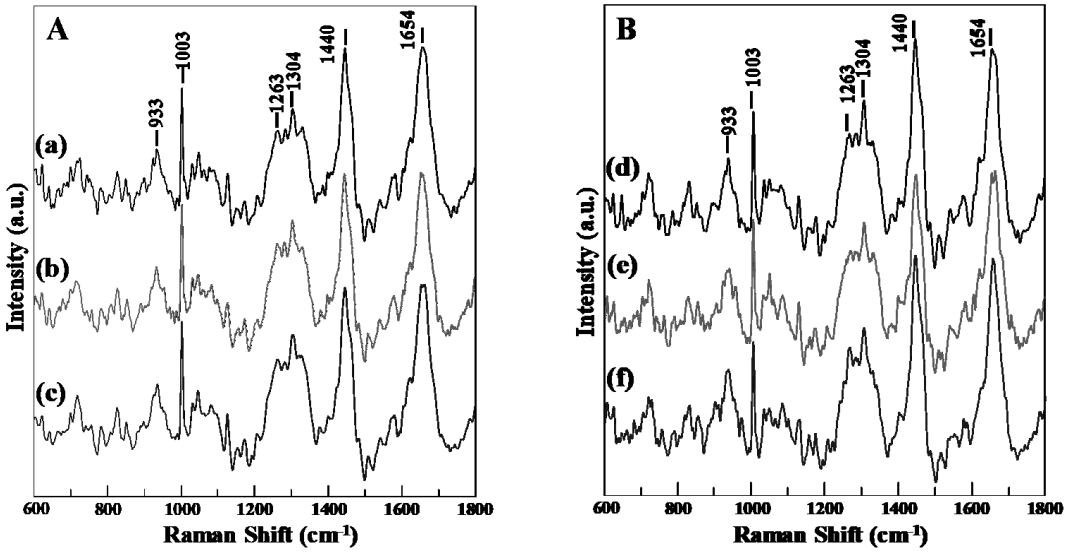

Fig.1-2 Raman spectra of tumors (averaged) measured in 3 tumor models, at 15 (a and d), 17 (b and e), and 19 (c and f) weeks of age (tumor model: 15 weeks, n = 19; 17 weeks, n = 24; 19 weeks, n = 19; control: 15 weeks, n = 7; 17 weeks, n = 9; 19 weeks, n = 7)

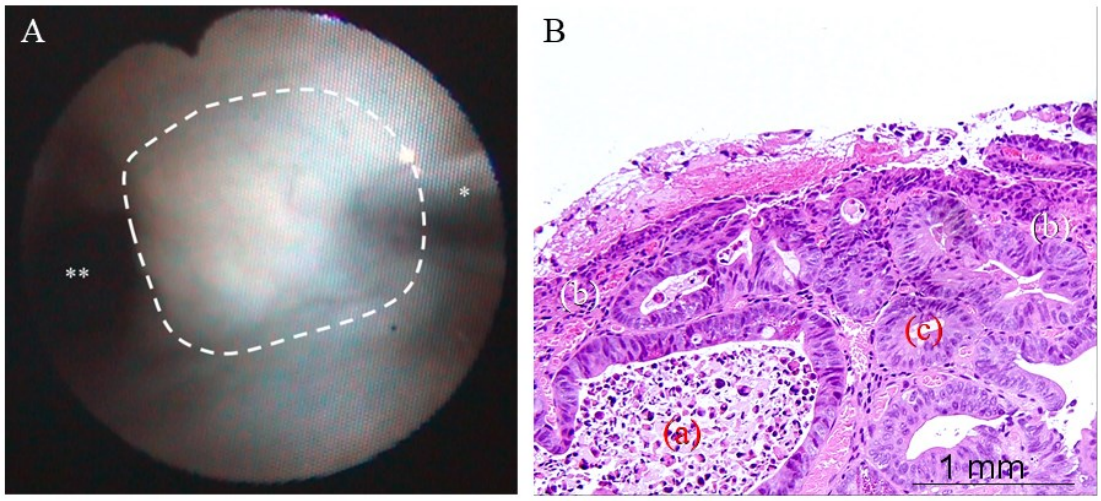

Fig.1-3 (A) photograph of a typical colon tumor measured with the endoscope in a 15 week old live model mouse, the tumor is marked with a broken line (---), the distance of the tumor from the anus is ±14 mm, the head of the BHRP (*) and the lumen of colon (**) are seen in the picture; (B) photomicrograph of a hematoxylin–eosin-stained colorectal adenocarcinoma in Fig. 1-3 A(---), the tissue was collected from a killed mouse (19 weeks old) and necrotic tumor cells (a), cancer cells (b), and normal cells (c) can be seen.

to the difficulty of deeply inserting the endoscope without scratching the vulnerable tumor

lesion. I selected 4 of 16 mice that have the best tumor configuration (i.e., the tumor has an easy-to-access location and is easily recognizable for continued endoscopic observation) for further observation. The head part of the endoscope could be bent up and down with a lever at its handle. The handle is rotated to turn the sight into either the right or the left direction. To point the probe toward a closer or farther tissue, the probe rod is pulled or pushed. With these simple manipulations, it is possible to reach any point within the colon through the visual guide of a TV monitor. A typical endoscope picture of a colon tumor in the mouse model is shown in Fig. 1-3A. The distal end of the BHRP can be seen at the right side of the sight. Generally, several (3–7) polyp-shaped tumors were observed in each mouse. A photomicrograph of an H/E-stained adenocarcinoma tissue is shown in Fig. 1-3B, which indicates that the tumor in the AOM/DDS mouse model has advanced into the malignant state. The tissue sample was obtained from a large polyp-like dysplasia. On the basis of our histopathologic examinations, an estimated 5–10% of tumors in the 20 week old mice are adenocarcinoma and the other tumors are adenoma.

2. Analysis of Raman spectra from colorectal tumors in model mice

The Raman spectra of live tumor model and control mice are shown in Fig. 1-2. I selected several polyp-like tumors in the 3 model mice and the measurements were repeatedly carried out at 15, 17, and 19 weeks of age (7th, 9th and 11th weeks after the administration of AOM). Several spectra were collected from different polyps in each model mouse and they were collected from different positions in the colon wall for the control mouse. The total numbers of the measured spectra were 19, 24 and 19 for 15 (a), 17 (b) and 19 (c) weeks of tumor models and 7, 9 and 7 for 15 (d), 17 (e) and 19 (f) weeks of control. The Raman spectra were analyzed with PLSR analysis The PLSR score plot

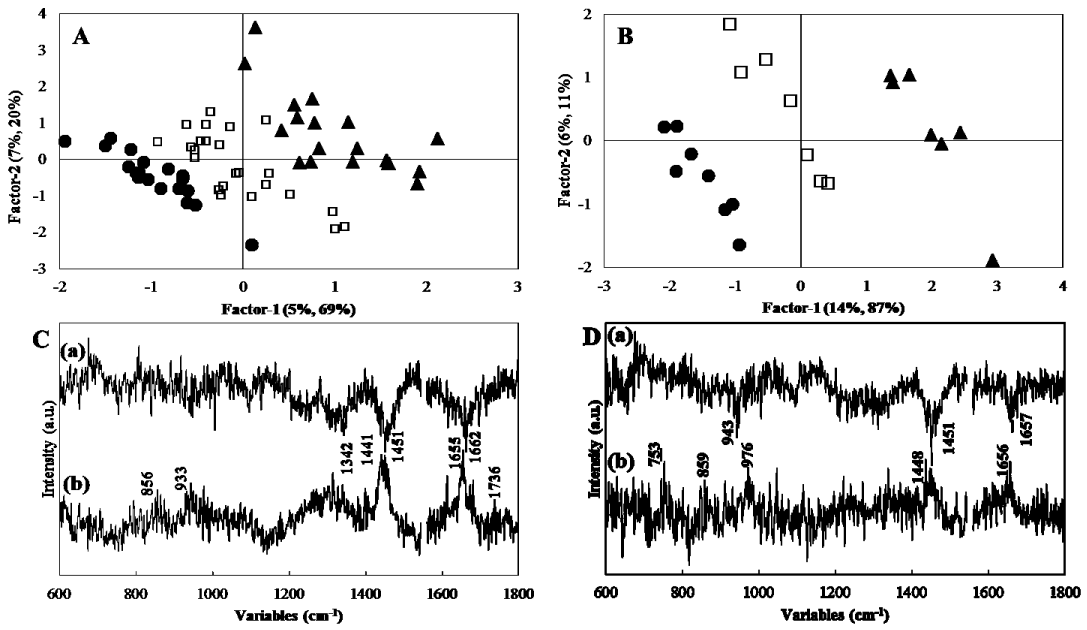

Fig.1-4 Score and loading plots for factors 1 and 2 of PLSR models obtained for the spectra measured in 3 tumor mouse models (A and C) and in a single tumor mouse model (B and D). Marks of ●, □ and ▲ represent the spectral data measuread at 15, 17, 19 weeks of age, respectively. The Raman spectra weremeasured at several tumor lesions in the mouse; for the 3 tumor mouse models, the total number of spectra are 19, 24 and 19 for 15, 17 and 19 weeks, for the single tumor mouse model, the total number of spectra are 8, 7 and 7 for 15, 17 and 19 weeks.

and loading plot for factors 1 and 2 calculated for 3 tumor mice are shown in Fig. 1-4A and C. The dataset is classified into 3 groups according to the number of weeks. The bands at 1662, 1451, and 1342 cm^{-1} are assigned to amide I, C-H bending, and amide III vibrational modes of protein in factor 1, and the bands at 1736, 1655, and 1441 cm^{-1} were assigned to C=O stretching, C=C stretching and C–H bending modes of triacylglycerol in factor 2, respectively. This tendency is observed more clearly in the PLSR score plot calculated for a single mouse. The score and loading plots of the spectra obtained from one mouse alone are shown in Fig. 1-4B and D. These score plots indicate that molecular alterations occurred as the tumor advanced. The results suggest that the tumor developed in one direction and all tumors showed a relatively uniform

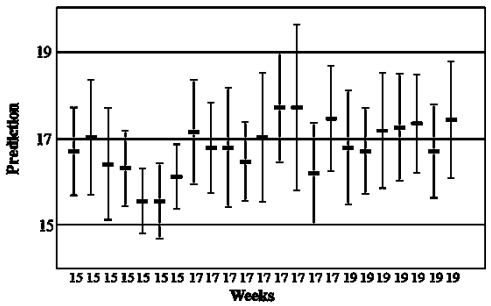

Fig. 1-5 Prediction result of the dataset of the control mouse (15 weeks n = 7, 17 weeks n=9, 19 weeks n = 7) applied to the PLSR model. Bars (-) represent prediction values and vertical bars do represent deviations of the prediction values.

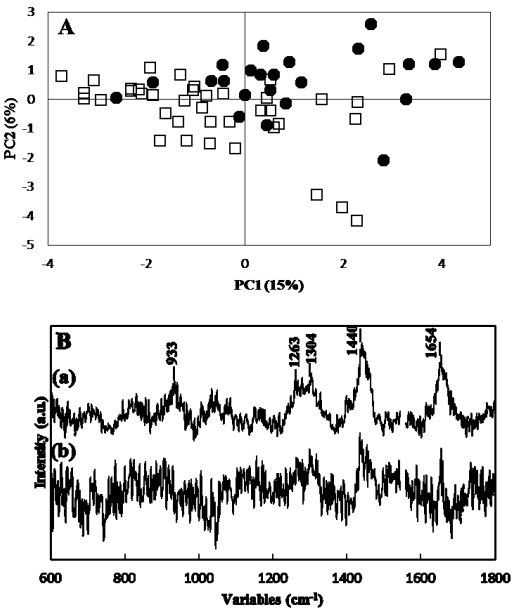

Fig.1-6 Score plot (A) for PC1 and 2 of a PCA model built for the Raman spectra obtained from control (● ; n = 22) and tumor (□ ; n = 41) mice, and loading plots (B) of PC1 (a) and 2 (b)

phase of development in the AOM/DSS mouse model. The validation result of the spectra of the control mouse applied to the PLSR model obtained for the 3 tumor mice is depicted in Fig. 1-5. When the control data applied to the PLSR model obtained for the tumor advancing, the prediction result has no relationship with the weeks of mouse. If the PLSR model reflected the usual aging effect of the colorectal tissue, the data would be classified depending on the weeks. It is not the case. The result strongly suggests that the PLSR model of the tumor mice successfully extracted specific information to the tumor progression. Fig. 1-6 shows a PCA score plot (A) and loading plots (B; principal components (PCs) 1 (a) and 2 (b)) calculated for the spectra of the tumor lesion in 2 model mice (B and C; n = 41) and for the control mouse (N; n = 23). The spectra of these 3 mice, including data obtained at different ages (15–19 weeks), were analyzed together.

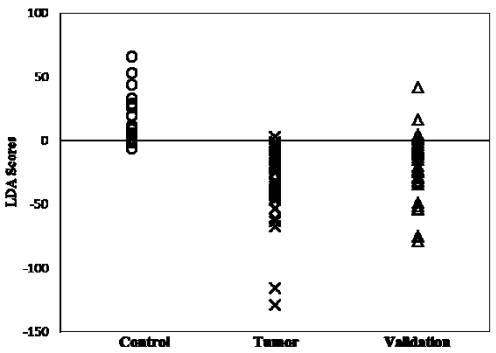

Fig.1-7 LDA score plot of the control dataset (○), tumor dataset (×), and validation dataset (△).

Strong five bands appeared at 1654, 1440, 1304, 1263, and 933 cm^{-1} in the loading plot of PC1 in Fig. 1-6B (a), which seemed to be assignable to lipids. I have inspected score plots for PC1 to PC7; however, no clear classification, including the week dependency, was observed. It seems that PLSR can extract information more efficiently depending on the dependent variables. Judging from the features of the loadings, PC1 and 2 are mostly arising from the protein in the negative direction and fat (triacylglycerol) in the positive direction. This judging due to the bands at 1662, 1451, and 1342 cm^{-1} is assigned to amide I, C-H bending[23], and amide III vibrational modes of protein[24] in PC1. Meanwhile, the bands at 1736, 1655, and 1441 cm^{-1} were assigned to C=O stretching[25], C=C stretching[26], and C–H bending modes of triacylglycerol[27] in PC2. The PCA score plot (A) and loading plots (B; PC1 and 2) in Fig. 1-6 were calculated for the spectra of model and control mice. Although the control and tumor spectra were not discriminated in the score plot, the spectra of the control mouse showed a tendency to have a larger PC1 contribution. Five bands strongly appeared at 1654, 1440, 1304, 1263, and 933 cm^{-1} in the loading plot of PC1, which seemed to be assignable to lipids. The result suggests that the normal colon tissue has a higher lipid concentration than the tumor. The data of the normal mouse and those of the tumor model mice were then analyzed with LDA. The LDA score plot is depicted in Fig. 1-7. The LDA model was constructed for the spectra of control (N; n = 23) and tumor mice (B and C; n = 41). The spectra of different tumor model mice (A and D; n = 38)

were used to validate the model. LDA was applied to the sample data with these 5 bands. The result showed that 86.8% (n = 33) of tumor samples were classified correctly and 13.2% (n = 5) incorrectly. Since all of the control data were used to obtain a reliable model, there is no control spectra left for validation. The validation is made with the spectra of different tumor model mice which were not used to build the model. Therefore, the present LDA model is relatively robust. Fig. 1-8A depicts a series of pictures of a shrinking tumor in the same mouse. These are endoscopic pictures observed at the same position in a model mouse at 15, 17, and 19 weeks of age. A small tumor is visible in the first picture (Fig. 1-8A(a)), slightly larger tumor appeared in the second picture (Fig. 1-8A(b)), and then in the third picture (Fig. 1-8A(c)) these tumors disappeared. The observed point was at 14 mm from the anus. Although a few tumors showed a reduction in size (shrinking tumors) during the observation, I have succeeded in simultaneously recording both pictures and spectral data in only one case because this was not a predictable phenomenon. In this case, the tumor seemed to have disappeared; however, the other tumors were only reduced in size. The shrinking tumors were generally small; however, no characteristic feature was recognized from the visual observation. The Raman spectra of this lesion are shown in Fig. 1-8B. The spectra of the shrinking tumor measured at 15 (Fig. 1-8B(a)), 17 (Fig. 1-8B(b)), and 19 (Fig. 1-8B(c)) weeks are depicted. The spectra in Fig. 1-8B(d) and (e) are the subtraction results of the 17 week spectrum minus the 15 week spectrum and the 19 week spectrum minus the 15 week spectrum, respectively. The spectra of the shrinking tumor measured at 15 (Fig. 1-8B(a)), 17 (Fig. 1-8B(b)), and 19 (Fig. 1-8B(c)) weeks showed similar features to those of the growing tumors shown in Fig. 1-3. The subtraction spectrum in Fig. 1-8B(d) shows a negative band at 933 cm^{-1}, which may be arising from collagen type I[28] and may indicate the less-

activity of tissue repair. Since the spectra were too noisy to collect information with visual comparison, the previous LDA model was applied for

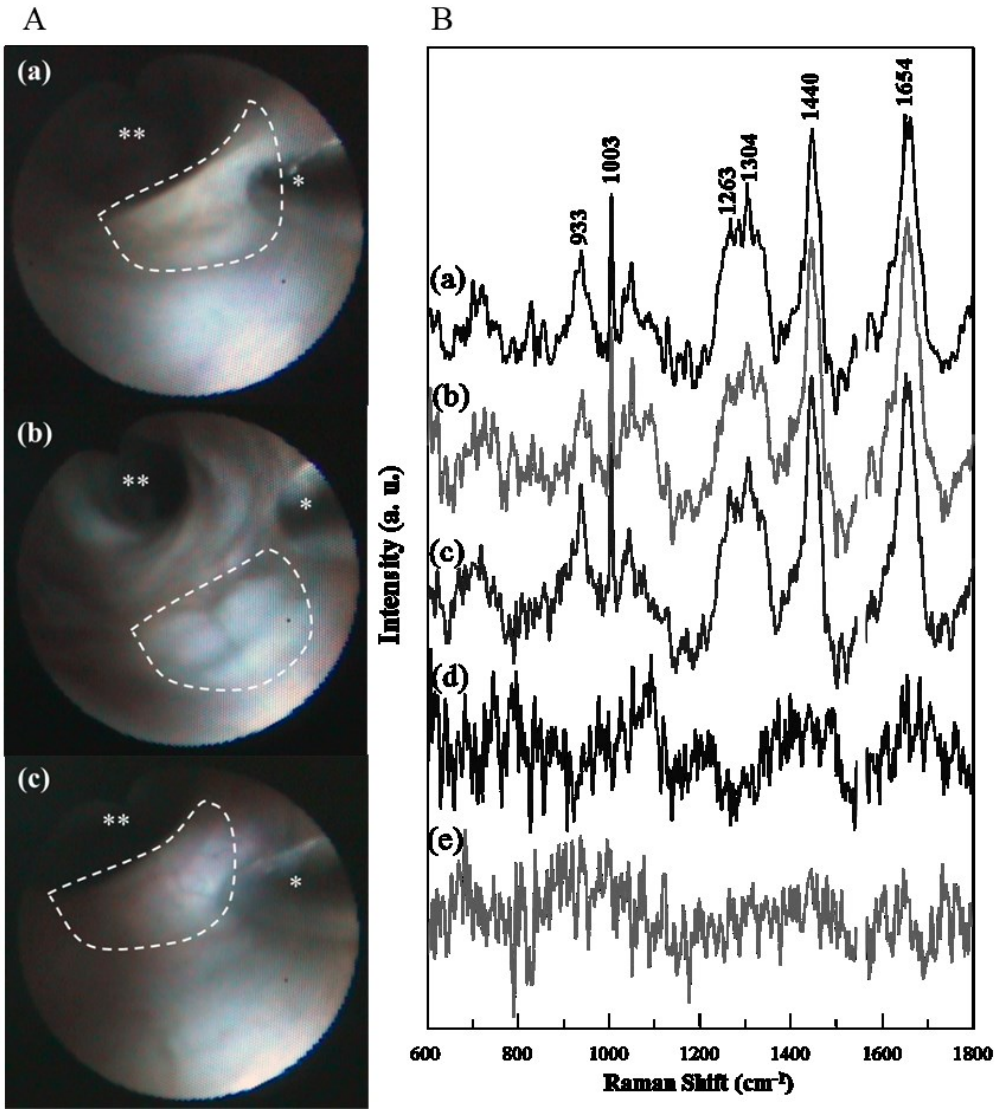

Fig.1-8 The pictures of shrinking tumor (A; 14 mm from anus) taken at mouse ages of 15 (a), 17(b) and 19(c) weeks; the Raman spectra of tumors (B; averaged) measured at mouse ages of 15 (a), 17 (b), and 19 (c) weeks, and the subtractions spectra of 17 weeks minus 15 weeks (d) and 19weeks minus 15 weeks (e). The spectra in the 1545-1559 cm^{-1} range were hidden to remove a strong noise due to the oxygen in the hollow fiber. The tumor is shown with dotted line (---). The head of the BHRP was marked by "*". The lesion with a "**" mark indicates the lumen of the colon.

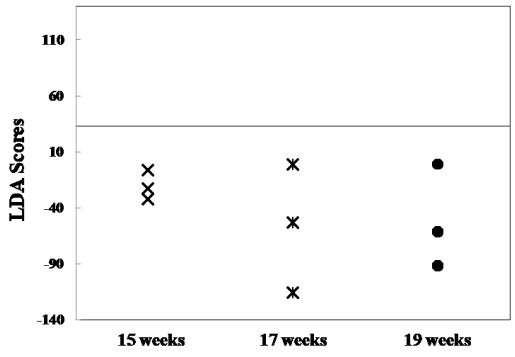

Fig.1-9 LDA score plot of the 15 weeks dataset (×), 17 weeks dataset (*), and 19 weeks dataset (●) of shrinking tumor.

diagnosis. Fig. 1-9 is the LDA score plot of the 15 weeks dataset (×), 17 weeks dataset (*), and 19 weeks dataset (●) used by LDA model in Fig.1-7. The spectra of the shrinking tumor were classified as "tumor" in Fig.1-9. It suggested that the shrunken tumor was disappeared by observation but Raman spectroscopy found the tumor. However, the shrunken tumor were not checked up and diagnosed by histopathologists due to unable to recognize the exact position of the shrunken tumor after sacrificed.

I - 5. Discussion

Observation and measurement of Raman spectra in individual mice were carried out repetitively during a 2 weeks interval to prevent the adverse effects of anesthesia. After the observation at 19 weeks, the mice were sacrificed for histopathological studies. Cautious observation of the extracted colon as well as endoscopic observation indicated that the Raman measurements with 60 mW laser irradiation did not cause any damage to the tissue. Not only the low level of laser irradiation, but the exposure time of laser was short enough, which did not cause the accumulation of energy to be hot and consequently give effect to the tissue. The laser irradiation level and exposure time will have a relationship with the damage of tissue[23]. Furthermore, pathologic analysis of the biological effects of laser–tissue interaction needs a relationship of the irradiation parameters with the biologic status and response of the target tissue over time[29].

Visual observation indicated that the tumors mostly grew in size during the 4 weeks but no other obvious changes were observed. Bands at 1654, 1440, 1263, and 1003 cm^{-1} were assigned to the amide I, C–H bending, and amide III vibrational modes of protein, and a breathing mode of the phenyl ring of phenylalanine[30], respectively. It seemed that a band at 933 cm^{-1} can be assigned to proline in collagen type I[31,32]. As the bands at 1654, 1440, and 1304 cm^{-1} seemed to have trace contributions of a lipid[24,33]. The working distance and the size of the focal volume were 60 and 58 μm the depth direction, respectively[9]. The tumor part is usually much thicker due to the dysplasia as shown in Fig. 1-1C. The lipid seems to be included in the tumor tissue itself.

The present study demonstrates that an *in vivo* study with a miniaturized Raman probe and a miniaturized endoscope is a powerful method for obtaining molecular and morphological information of tissues in real time without damaging the tissue. Although no bleeding occurred during the operation, the anesthesia procedure is still necessary for studies with this colorectal tumor mouse model. From this viewpoint, although introducing the endoscope may be a semi-noninvasive method, the procedure might still cause pain to the animals. The possibility of monitoring unique alterations in the molecular composition of the colorectal tumor will allow us to study the therapeutic effects of not only anticancer drugs but also various medical treatments, using individual model mice. The technique may also contribute to reducing the number of mice to be killed in studies. The tumor grade was not discussed in this study because I focused on the noninvasive observation of the tumors. It was possible to conduct a biopsy for a part of the tissue with forceps; however, it might cause severe inflammation, infection, and irregular tissue formation during repair. The present results reveal that the molecular composition of a tumor changes as the tumor advances.

This kind of study would be very difficult to use other tumor animal models such as the dog or sheep model because it would take a long time to create the model and to advance the tumor in these medium-sized animals. Although the mouse model is too small for the commercially available endoscopes, it has the advantage of ease in preparation and tumor control. The present system allows the use of a mouse model to study the molecular alterations and the morphology of live tumor tissues continuously.

I - 6. Conclusion

The present study demonstrated that this Raman system equipped with a miniaturized endoscope and BHRP can simultaneously obtain spectral and visual information on the same tumor in a single mouse through continued measurements for several weeks. The results of Raman monitoring of tumors suggested some biochemical alterations in the molecular composition of the tumor, such as the change in the concentration of collagen type I and lipids in the lesion. The LDA model was constructed with 5 bands mainly assigned to lipids distinguishing the tumor and the control tissues. I have succeeded in observing and measuring the Raman spectra of a shrinking tumor. According to the LDA analysis, the shrinking tumor was not cured but rather transformed to another tumor type. The animal test using a mouse is irreplaceable for the basic research of tumor. The present technique can contribute to open a new era into the advanced mouse model research.

I - 7. Acknowledgements

This study was financially supported by Konica Minolta Technology Center and A-step, JST (Japan Science and Technology Agency).

I - 8. References

1. Cancer statistics in Japan, *FPCR National Cancer Center*, 2015
2. M. Hollstein, D. Sidransky, B. Vogelstein and CC. Harris, *Science*, 1991, **253**, 49-53
3. M. G. Havenith, J. W. Arends, R. Simon, A. Volovics, T. Wiggers and F. T. Bosman, *Cancer*, 1988, **62**, 2207-2211
4. K. W. Kinzler and B. Vogelstein, *Cell,* 1996, **87**, 159–170
5. T. Takayama, S. Katsuki, Y. Takahashi, M. Ohi, S. Nojiri, S. Sakamaki, J. Kato, K. Kogawa, H. Miyake and Y. Niitsu, N. Engl. *J. Med.*, 1998, **18**, 1277-1284
6. M. S. Bergholt, W. Zheng, K. Lin, K. Y. Ho, M. Teh, K. G. Yeoh, J. B. Y. So and Z. Huang, *Analyst*, 2010, **135**, 3162–3168
7. M. S. Bergholt, W. Zheng, K. Lin, K. Y. Ho, M. Teh, K. G. Yeoh, J. B. Y. So and Z. Huang, *J. Biomed. Opt.*, 2011, **16**, 037003.
8. A. S. Haka, Z. Volynskaya, J. A. Gardecki, J. Nazemi, R. Shenk, N. Wang, R. R. Dasari, M. Fitzmaurice and M. S. Feld, *J. Biomed. Opt.*, 2009, **14**, 054023.
9. F. Zheng, Y. Qin and K. Chen, *J. Biomed. Opt.*, 2007, **12**, 034002.
10. Y. Hattori, Y. komachi, T. Asakura, T. Shimosegawa, G. Kanai, H. Tashiro and H. Sato, *Appl. Spectrosc*., 2007, **6**, 579–584
11. Y. Komachi, T. Katagiri, H. Sato and H. Tashiro, *Appl. Opt*., 2009, **48**, 1683–1696
12. Y. Komachi, H. Sato, K. Aizawa and H. Tashiro, *Appl. Opt.*, 2005, **44**, 4722–4732
13. T. Katagiri, Y. S. Yamamoto, Y. Ozaki, Y. Matsuura and H. Sato, *Appl. Spectrosc*., 2009, **63**, 103–107
14. Y. S. Yamamoto, Y. Oshima, H. Shinzawa, T. Katagiri, Y. Matsuura, Y. Ozaki and H. Sato, *Anal. Chim. Acta,* 2008, **619**, 8–13
15. B. B. Andriana, M. Norio, M. Atsushi, A. Toru, K. Masamichi and H. Sato, in *In hope*

of going over the present Clinical PD and PDT, ed. N. Miyoshi and R. H. Pottier, Sankeisha Co., Ltd., Japan, 2011, pp. 97–112

16. D. W. Rosenberg, C. Giardina and T. Tanaka, *Carcinogenesis*, 2009, 30, 183–196
17. A. I. Thaker, A. Shaker, M. S. Rao and M. A. Ciorba, JoVE, 2012, **11**, 4100.
18. C. Becker, M. C. Fantini, S. Wirtz, A. Nikolaev, R. Kiesslich, H. A. Lehr, P. R. Galle and M. F. Neurath, *Gut*, 2005, **54**, 950–954
19. C. Constantinides, R. Mean and B. J. Janssen, *ILAR J.*, 2011, **52**, e21–e31
20. B. B. Andriana, Y. Oshima, S. Takanezawa, T. W. Tay, C. L. R. Soeratman, M. S. Alam, H. Mitsuoka, X. B. Zhu, T. Suzuki, Y. S. Yamamoto, N. Tsunekawa, Y. Kanai, M. Kurohmaru and H. Sato, BiOS-SPIE, San Jose, California, USA, 2009, 7167-33.
21. Y. Oshima, H. Shinzawa, T. Takenaka, C. Furihata and H. Sato, *J. Biomed. Opt*., 2010, **15**, 017009.
22. Y. Oshima, H. Sato, A. Zaghloul, G. N. Foulks, M. C. Yappert and D. Borchman, *Curr. Eye Res.*, 2009, **34**, 824–835
23. R. J. Lakshimi, V. B. Kartha, C. M. Krishna, J. G. R. Solomon, G. Ullas and P. U. Devi, *Radiat. Res*., 2002, **157**, 175–182
24. C. Kraft, L. Neudert, T. Simat and R. Salzer, *Spectrochim. Acta, Part A*, 2005, **61**, 1529–1535
25. I. Notingher, C. Green, C. Dyer, E. Perkins, N. Hopkins, C. Lindsay and L. L. Hench, *J. R. Soc., Interface*, 2004, **1**, 79–90
26. R. Malini, K. Venkatakrishma, J. Kurien, K. M. Pai, L. Rao, V. B. Kartha and C. M. Krishna, *Biopolymers*, 2006, **81**, 179–193
27. L. Silveira, S. Sathaiah, R. A. Zangaro, M. T. T. Pacheco, M. C. Chavantes and C. A. G. Pasqualucci, Lasers *Surg. Med*., 2002, **30**, 290–297.

28. W. T. Cheng, M. T. Liu, H. N. Liu and S. Y. Lin, Microsc. *Res. Tech*., 2005, **68**, 75–79

29. S. Thomsen, *Photochem. Photobiol*., 1991, **53**, 825–835

30. J. W. Chan, D. S. Taylor, T. Zwerdling, S. M. Lane, K. Ihara and T. Huser, *Biophys. J.*, 2006, **90**, 648–656

31. I.Notingher, I.Bisson, A. E. Bishop,W.L.Randle, J.M. P. Polak and L. L. Hench, *Anal. Chem.*, 2004, **76**, 3185–3193

32. H. U. Gremlich and B. Yan, Infrared and Raman spectroscopy of biological materials, *New York*, 2001, pp. 421–476

33. N. Stone, C. Kendall, J. Smith, P. Crow and H. Barr, Faraday *Discuss*., 2004, **126**, 141–157

Chapter II : Raman Endoscopy for Monitoring Anticancer Drug Treatment of Colorectal Tumors in Live Mice

II - 1. Abstract

I have developed a murine model to study the effects of anticancer treatment on colorectal tumors. A miniaturized Raman endoscope (mRE) system was employed for the study. The endoscope is narrow enough to observe the inside of the mouse colon under anesthesia. It has a channel for a ball lens mounted on a hollow fiber Raman probe (BHRP) to measure any targeted point under the visual control of the endoscope. Colorectal cancer tissue was observed to study alterations of the tissue in response to anticancer drug treatment. Three anticancer drugs, 5-fluorouracil (5-FU), cisplatin (CDDP), and docetaxel were employed. Although no alteration was recognized in the endoscopic visual observations at 2 weeks after the drug treatments, the Raman spectra obtained in the live mouse colon indicated that changes of lipids and proteins were observed. This study demonstrates that *in situ* Raman analysis is powerful in detecting the effects of anticancer drugs.

II - 2. Introduction

Colorectal cancer is the third most cancer death in men and first most cancer death in women in Japan[1] and anticancer drugs are a mainstay in treating any cancer. There are many kinds of anticancer drugs but they can cause severe side effects. Therefore, it is necessary to select the most effective drugs for each case while limiting side effects. This is not straightforward because of the individual characteristics of each cancer. During chemotherapy, higher doses are preferable to destroy cancer cells but the dosage may need to be limited in order to minimize side effects[2]. In clinic, selection of cancer drugs is based on doctor's experience and knowledge[3]. The selected drugs have to work greater efficiency and lower toxicity for patients[4].

The purpose of the present study was to develop a technology to estimate the efficiency of anticancer drugs over short periods of time. For this purpose, I applied Raman spectroscopy via endoscope to evaluate the effects of different anticancer drugs in a noninvasive manner. It is difficult to do this with repeated biopsies because of their invasive character. For continuous measurement of responses, minimally invasive methodologies are required. Raman spectroscopy provides information about the molecular composition without damaging the tissue (i.e., noninvasively)[5]. I used the azoxymethane-dextran sodium sulfate (AOM-DSS) colon cancer mouse model because the tumor progresses very rapidly and only 1 month is needed for sample preparation. Such a model is easily manipulated, allowing a well-controlled environment for cancer research[6].

Raman spectroscopy has been applied to explore the implications of early cancer detection in the human stomach during clinical gastroscopy, which led to the development of a 1.8 mm Raman endoscopic probe for *in situ* measurements. Cancerous tissues can be

identified inside the stomach and esophagus with an accuracy of 89.3% and 94.7%, respectively[7]. Meanwhile, Raman endoscopy has been suggested for human breast cancer diagnosis (in an *ex vivo* study)[5]. This study reported a sensitivity of 83% and a specificity of 93% for the evaluation of freshly excised surgical specimens. For colorectal cancer diagnosis, it has been reported that the Raman analysis of single live epithelial cell had a sensitivity of 86.3% and a specificity of 86.3%[8].

This present study was to evaluate the effect of anticancer drugs in live colorectal cancer mouse models using a Raman endoscope system. We have developed a miniaturized Raman probe and an endoscope specifically for use in the mouse[7,9,10]. A ball lens-installed hollow optical fiber Raman probe (BHRP) consists of a sapphire ball lens and a hollow optical fiber[11,12]. The endoscope system allows the direct observation of the tumor in the colon. The colorectal cancer model is created through the administration of azoxymethane (AOM) and dextran sodium sulfate (DSS)[6]. Live tumor-bearing mice are then treated with one of three anticancer drugs, 5-fluorouracil (5-FU), cisplatin (CDDP), or docetaxel.

5-FU is an analog of uracil with a fluorine atom at the C-5 position instead of hydrogen. 5-FU is converted intracellularly to several active metabolites, including fluorodeoxyuridine monophosphate (FdUMP), fluorodeoxyuridine triphosphate (FdUTP), and fluorouridine triphosphate (FUTP); these active metabolites disrupt DNA and RNA synthesis and the action of thymidylate synthase (TS)[13]. CDDP interacts with DNA to form DNA adducts, primarily intra-strand crosslink adducts, which activate several signal transduction pathways, including those involving ATR, p53, p73, and MAPK, and culminates in the activation of apoptosis[14]. Docetaxel is a semisynthetic taxane. Docetaxel targets the β subunit of tubulin heterodimers, thereby stabilizing microtubules and

inducing cell-cycle arrest and apoptosis[15]. These drugs all disrupt cellular activity to interfere with the cell cycle and/or mitosis and induce cell death but their mechanisms are different.

Principal component analysis (PCA) was employed for the classification of the Raman spectra related to the anticancer drug treatment and control groups to detect tissue alterations in response to drug treatment. I hypothesized that Raman analysis would be able to discriminate the effects of these drugs based on the molecular compositional changes they induced.

Reactions of cancer cells to anticancer drugs have been studied *in vitro* using Raman imaging[16]. Cancer tissue consists of not only cancer cells but also extracellular matrix, and many other cells, e.g., macrophages and vascular endothelial cells. Among the various types of cells, cancer stem cells have tumorigenic capacity and their presence seems to closely correlate with tumor drug resistance[17]. Skolekova et al. reported that pretreatment of human mesenchymal cells with CDDP led to changes in the phosphorylation profiles of many kinases and also increased secretion of IL-6 and IL-8 cytokines, which increased the chemoresistance and stem cell characteristics of breast cancer cells[18]. In addition, high collagen content in a tumor's extracellular matrix and its organization into a thick fibrous network, particularly in poorly vascularized hypoxic regions, increase tissue stiffness, providing an additional physical barrier that further limits the penetration of anticancer drugs[19]. These reports suggest the importance of research on whole cancer tissue at the molecular level. The endoscope with Raman spectroscopy gives us a chance to study intact cancer tissue with repeated non-invasive observations during long term chemotherapy. The present study demonstrated the feasibility of Raman endoscope in the study of anticancer drugs *in situ*.

II - 3. Material and Methods

1. Preparation of the AOM-DSS colorectal cancer model mice

BALB/cCrSlc mice were purchased from SLC (Shizuoka, Japan). The AOM and DSS were purchased from Sigma-Aldrich Chemical Co. (St. Louis, MO, USA). AOM was dissolved in normal saline solution (Otsuka Pharmaceutical Co., Ltd., Tokushima, Japan) and a 7.4 mg/kg dose was administered by intraperitoneal injection to each 8-week-old mouse[6]. The mice were then fed DSS in drinking water (30 mg/ml) for 1 week and this cycle was repeated twice at a 2-week interval. The study was approved by the ethics committee of Kwansei Gakuin University.

2. Anticancer drug treatment

5-FU (LKT Laboratories, Inc., Tokyo Chemical Industry, Tokyo, Japan), docetaxel (Tokyo Chemical Industry, Japan), and CDDP (Tokyo Chemical Industry, Tokyo, Japan) were the anticancer-drugs used. 5-FU and CDDP were diluted with saline in accordance with previous reports[20,21]. They were administered to the mice at doses of 25 mg/kg and 1.3 mg/kg for 5-FU and CDDP, respectively. The stock solution of docetaxel (50 mg/ml in ethanol) was diluted with polysorbate 80 (Wako Pure Chemical Industries, Ltd., Osaka, Japan) and 5% dextrose (Sigma-Aldrich Chemical Co., St. Louis, MO, USA) in water (D5W) as described in previous reports[22]. The prepared solutions were administered by intravenous injection 2 weeks after AOM/DSS treatment and Raman measurements were then carried out 2 weeks after the anticancer drug treatments. Control mouse models were treated with normal saline instead of anticancer drugs. There were five 5-FU, three CDDP, three docetaxel treated and two control AOM/DSS mouse models prepared. Three of the 5-FU treated models underwent Raman observation before

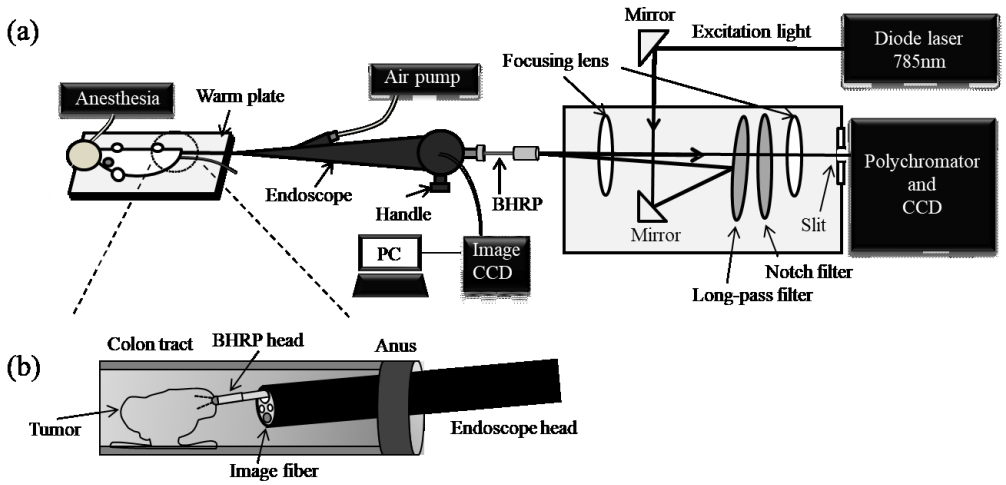

Fig.2-1 The structure of the miniaturized Raman endoscopic system with a schematic drawing of the experimental setup (a); the structure of the head of the endoscope and image of the Raman measurement in a colon tumor (b).

and after the drug treatments. CDDP and docetaxel treated models didn't observed before and after treatments. All chemicals used were reagent, not medical, grade.

3. Raman measurements

A Raman system equipped with BHRP and a miniaturized endoscope were used for *in situ* Raman measurement in the live mouse colon[11,12]. The endoscope (Machida Endoscope Co. Ltd., Japan) had a 1.2 mm diameter channel for the BHRP, illumination, and image fibers, and its total diameter was 2.5 mm. The BHRP had a sapphire ball lens 500 μm in diameter (Edmund Optics, USA) and a hollow optical fiber of 420 μm outer diameter (Doko Engineering LLC, Japan)[9-12]. A diode laser (785 nm, Toptica Photonics, Germany) was used for excitation. The Raman system included a single polychromatic Raman spectrometer (F4.2, focal length 320 mm, 750 nm blazed 600 l/mm grating; Photon Design Co. Ltd., Japan) and a charge coupled device detector (DU420-BRDD; Andor Technology Co. Ltd., Northern Ireland). The BHRP was coupled to the spectrometer through a long-pass filter (LF; Semrock, USA), a notch filter (NF; Kaiser

Optical System, USA), and 2 lenses to focus the laser and Raman scattered light into the hollow optical fiber and the slit (100 μm width: ~10 nm of spectral resolution). Schematic pictures of the Raman system are depicted in Fig. 2-1. The detailed specifics of the instruments have been described elsewhere[23]. To obtain high quality Raman spectra, the laser power was 60 mW and the exposure time was 60 seconds.

4. Procedure for endoscopic observation

The mouse was anesthetized using an inhalation anesthesia apparatus (SurgiVet, USA) and kept on a warming plate to maintain body temperature[23]. The concentration of isoflurane (Mylan, Tokyo, Japan) was carefully controlled in the range between 1.0 and 2.5%. The endoscope was inserted into colon through the anus, and then the lumen was pressurized with air via the channel to maintain the field of view. Feces that remained in the colon were removed by washing with saline. The BHRP was inserted into the endoscope's channel to measure the Raman spectra. The distance of the tumor from the anus was recorded through repeated measurements. The detailed procedure for observation and measurement has been described previously[23].

5. Histology study

Mice were sacrificed under anesthesia after Raman measurement and the colon was resected. The colon tissue was fixed with 10% formaldehyde (Wako Pure Chemical Industries, Ltd., Japan) for 24 hours and dehydrated with ethanol. The tissue was sliced at 5 μm thickness after paraffin (Sakura Fineteck, Japan) embedding[25] and the samples were stained with Masson's trichrome stain HT15-1KT kit (Sigma-Aldrich Chemical Co., St. Louis, MO, USA) and Mayer's hematoxylin solution (Sigma-Aldrich Chemical Co.,

St. Louis, MO, USA) for histopathological study.

6. Data analysis

The Raman spectrum was treated to remove background noise spectra due to the Raman probe and the coupling stage. Then, fifth polynomial line fitting was applied repeatedly 5 times to remove any fluorescent background. To minimize negative composition in the spectrum, only spectral areas with a negative value were subjected to the fifth polynomial fitting from the second iteration. The spectral intensity was standardized with a phenylalanine band at 1003 cm^{-1}, which was sharp and helped to accurately determine the intensity accurately[26]. Chemometrics software (Unscrambler; CAMO, USA) was used for principal component analysis (PCA) and partial least square regression discrimination analysis (PLSR-DA)[27,28]. Spectrum smoothing was applied to remove noise using the Savitzky-Golay method (11 points) for the spectra shown in Fig. 2-3.

II - 4. Results

1. Observation of the same tissue before and after drug treatment

Mice with tumors that were too large were excluded from the study to avoid excess contact with the endoscope head. Since large tumor lesions are often vulnerable and easily scratched, I was concerned that physical stimulation may affect the characteristics of the tumor. The head part of the endoscope can be moved up and down through the use of a

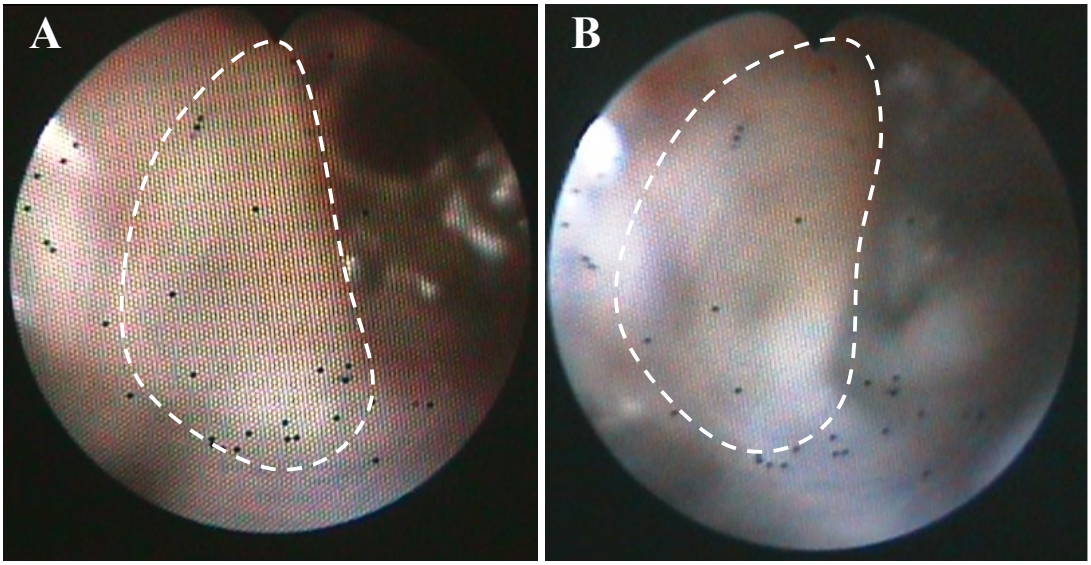

Fig.2-2 Endoscopic images of a typical colon tumor. An image before anticancer drug treatment (A; 15 weeks old) and after anticancer drug treatment (B; 17 weeks old).

lever at its handle. The probe rod is pulled or pushed gently to position the probe head at the measuring site. It was possible to reach any point within the lower colon and rectum under visual guidance. The detailed handling procedure has been described in our previous report[22]. Several (3–7) tumors were measured in each mouse model.

First, I investigated the effect of the anticancer drug on the same tumor in the 3 mouse models. Tumors were observed with the Raman endoscope; the mice were treated with the drug for 2 weeks, and then observed again with the Raman endoscope. Pictures of a typical colorectal cancer lesion before (A) and after (B) 5-FU treatment are shown in Fig. 2-2. No major difference was observed in shape, size, or color in the images. The effect of 5-FU cannot be determined by endoscopic observation. Corbett et al. reported that 5-FU treated colorectal tumor sizes in mouse are not different only two weeks[29]. The averaged Raman spectra of the tumors before (a; n = 24) and after (b; n = 22) the 5-FU treatment collected from the 3 mice, and their different spectra (c) are depicted in Fig. 2-3. Bands at 1654, 1440, and 1304 cm^{-1} were assigned to amide I, CH

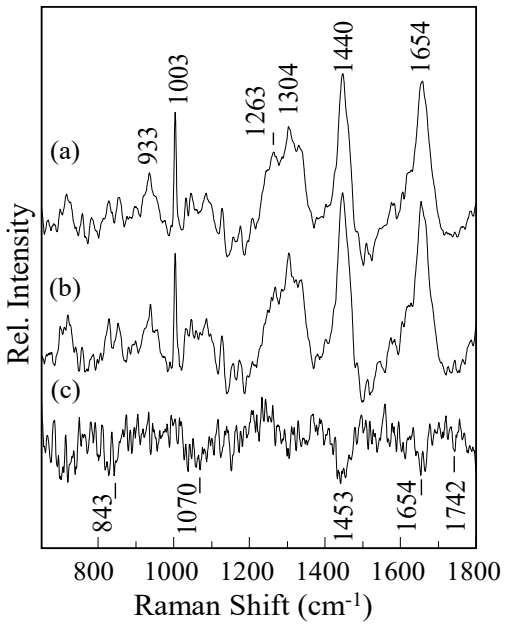

Fig. 2-3 Raman spectra of tumors measured before (a; n = 24) and after anticancer drug treatment (b; n = 22), and their different spectra (c; (b)–(a))

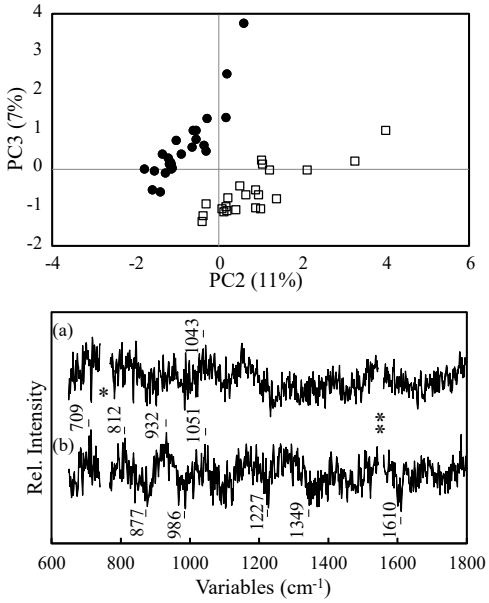

Fig. 2-4 A score plot (A) for PC2 and 3 of the PCA model built for the datasets of tumor tissue before (●; n = 24) and after 5-FU treatment (□; n = 22). Loading plots (B) of PC2 (a) and PC3 (b). (*: sapphire ball lens, **: oxygen)

bending, and amide III vibrational modes of the proteins[30]. Very weak bands appeared in the different spectrums (c) so their spectral difference was relatively small in the averaged spectra. The weak negative bands at 1742, 1453, 1070, and 843 cm^{-1} may be attributed to fat[31,32].

The spectra of tumors before and after the 5-FU treatment were analyzed with PCA. A score plot for PC2 and PC3 is depicted in Fig. 2-4A. The datasets of these groups are clearly classified into two distinct sets, suggesting that molecular alterations occurred due to drug treatment. Although data were obtained from 3 mice, no remarkable division or grouping was observed in each group for before/after drug treatment. This shows that the AOM/DSS treatment induced well-controlled oncogenesis and that this model generated homogeneous tumor tissues. The PC1 was strongly related to the presence of

fat and has no relevance to discrimination between the datasets (data not shown). The PC2 and 3 contributed almost equally to the discrimination. The contributions of PCs 1–3 were 19%, 11%, and 7%, respectively. There was no remarkable information included in PCs 4–8 to discriminate these 2 datasets. The loading plots of PC2 and 3 are shown in Fig. 2-4B. They show characteristic features in the wave number area below 1300 cm^{-1}. Since PCA merely extracts components related to the largest dispersion in the datasets, it is blind to the origin of the component. Because the PCs are orthogonal to each other, the loading plot of the lower PC is distorted by the higher PC. In the PCA result, a discriminating component between the 2 groups is divided into PC2 and PC3. To maximize the difference between the two data groups, PLSR-DA is applied. Two dependent variables, "−1" or "1" were assigned to the datasets before or after the treatment. Since each dataset was weighted according to the dependent variables, the factor in PLSR-DA generally represents the strongest contribution able to distinguish 2 datasets. The discrimination model was evaluated by the leave-one-out cross-validation method.

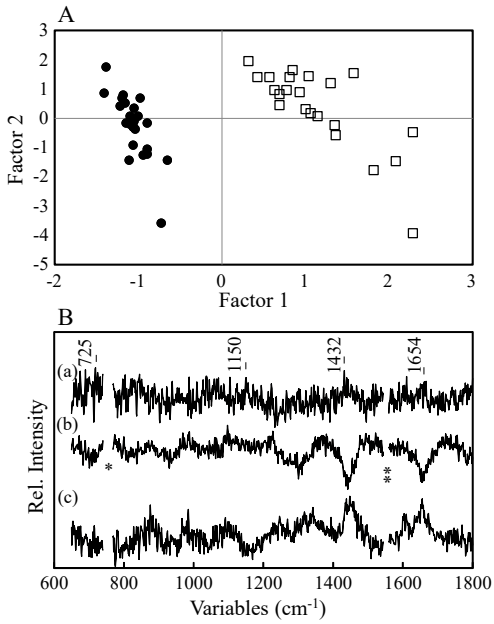

Fig. 2-5 A score plot (A) for factors 1 and 2 of the PLSR-DA model built for the datasets of tumor tissue before (●; n = 24) and after 5-FU treatment (□; n = 22). Loading plots (B) of factor 1 (a), factor 2 (b), and factor 3 (c). (*: sapphire ball lens, **: oxygen).

A score plot for factors 1 and 2 is depicted in Fig. 2-5A. The datasets were successfully categorized, particularly due to factor 1. The correlation coefficients for the

calibration and validation were 0.974 and 0.904, respectively, for the discrimination model built with 3 factors. The loading plots of factors 1–3 are shown in Fig. 2-5B and represent the largest differences between these two data groups. Although it is noisy, there are several positive broad bands near 1654, 1432, 1150, and 725 cm^{-1} observed in factor 1. They seem to correlate with saccharides, DNA, RNA, and some amino acids in the tissue[33]. Factors 2 and 3 seem to reflect changes in protein components. According to a previous study, the concentration of collagen I was reduced along with the advancement of the tumor[24]. However, characteristic bands due to collagen were not observed in the factors. All data were obtained from the same tumor in the same mouse, and therefore the results exclude lesion dependency and mouse dependency but include time dependency; there was a 2-week difference between the data acquisitions for with and without anticancer drug treatment.

2. Comparison of effects among 3 anticancer drug treatments

The effects of 5-FU, CDDP, and docetaxel were compared in the same age AOM/DSS mouse models. To study the effect of anticancer drugs free from time dependency, a separate control mouse model that was the same age as the drug-treated model and did not undergo any drug treatment was employed. The Raman spectra are not shown here but were very similar to the spectra of the tumor in Fig. 2-3. Since the different spectra between the treated and control groups did not provide much useful information, the Raman spectra were analyzed with PCA and PLSR-DA. The datasets of the 2 control and 5-FU treated 3 mice had separated groups in a score plot for PC1 and PC3. There is

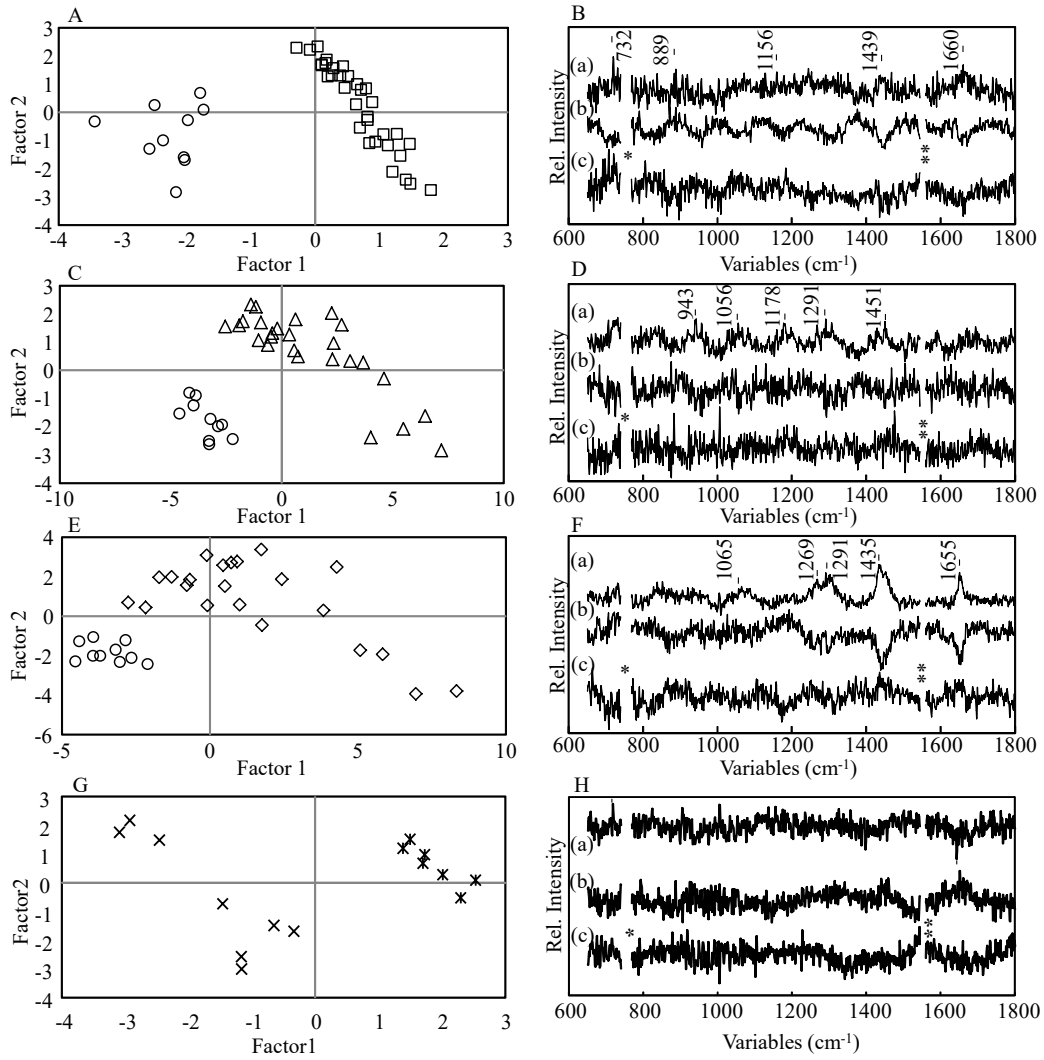

Fig. 2-6 Score and loading plots of the PLSR-DA model built for tumor lesions without and with treatments with 5-FU (A, B), CDDP (C, D), and docetaxel (E, F). Figures A, C, and E represent their score plots for control (no treatment; ○; n = 10), 5-FU (□; n = 32), CDDP (△; n = 26), and docetaxel (◇; n = 22). Figure G represent score plots for control (no treatment; ×; n = 8) and control (no treatment; ＊; n = 7). Figures 2-6B, 6D, 6F and 6H are loading plots of their factor 1 (a), factor 2 (b), and factor 3 (c). (*: sapphire ball lens, **: oxygen)

no obvious information to distinguish the data groups observed in PCs 2 and 4–8. As a results of analysis only one group for checking individual difference by PCA, the data from 5-FU treated 3 mice was not separated in PC1 to PC7 and the data from 2 control mice was not separated in PC1 to PC7, too. Intra-category classification was not observed

in both the control and treated datasets, suggesting that there is no characteristic or individual difference among the mouse models. The PLSR-DA results are shown in Fig. 2-6. A score plot for factors 1 and 2 for the datasets of 5-FU treated and control cancer mouse models is depicted in Fig. 2-6A. The data groups are categorized into 2 groups mainly according to factor 1. Loading plots of factors 1–3 are shown in Fig. 2-6B. The correlation coefficients of the discrimination model were 0.982 and 0.851 for the calibration and validation for the discrimination model built with 3 factors, respectively. Several positive broad bands were observed near 1660, 1439, 1156, and 732 cm^{-1} in factor 1, similar to those in factor 1 in Fig. 2-5B.

Reactions of the tumors to different kinds of anticancer drugs were observed. PLSR-DA results for datasets of control and CDDP treated mouse models are shown in Fig. 2-6C and 2-6D. The correlation coefficients were 0.975 and 0.765 for the calibration and validation for the discrimination model built with 3 factors. The control and treated datasets are well discriminated in the score plots for factors 1 and 2 (Fig. 2-6C). These 2 factors suggest that there are at least 2 independent reactions taking place in the tumor tissue due to CDDP administration. Loading plots of factors 1–3 are depicted in Fig. 2-6D. The spectrum has no apparent features, suggesting that the loading plot reflects minor alterations within molecular species, such as lipids and proteins, but not large increases or decreases of specific molecules. PLSR-DA results for the datasets corresponding to control and docetaxel treated mouse models are depicted in Fig. 2-6E and 2-6F. The correlation coefficients of the discrimination model were 0.967 and 0.709 for the calibration and validation for the discrimination model built with 3 factors. The control and treated datasets are also well discriminated in the score plot for factors 1 and 2 (Fig. 2-6E). Loading plots of factors 1–3 are depicted in Fig. 2-6F. Bands at 1655, 1435, 1291,

and 1269 cm^{-1} are assigned to C=C stretching, CH deformation, CH_2 bending, and C-H bending vibrational modes of lipids, respectively[34-36]. The spectral features of factors 1 and 2 looks like they correspond to fat. There are some broad bands observed in the lower frequency region that reflect differences in hydrocarbon chain length. The drug treated data group has minus scores in both factors 1 and 2. In contrast, the loading plots are positive for factor 1 but negative for factor 2. These facts suggest exchanges of fat species for those that may have different chain lengths. Lipids may leak out from the cells by apoptosis and be reflected in the measurement. PLSR-DA results for the data sets corresponding to control and control mouse models are depicted in Fig. 2-6G and 2-6H for negative control. The correlation coefficients of the discrimination model were 0.997 and 0.601 for the calibration and validation for the discrimination model built with 3 factors. Loading plots of factors 1–3 are depicted in Fig. 2-6H. No characteristic band appears in loading plots of factor 1-3 in Fig. 2-6H. These facts suggest almost noise factor discriminate controls.

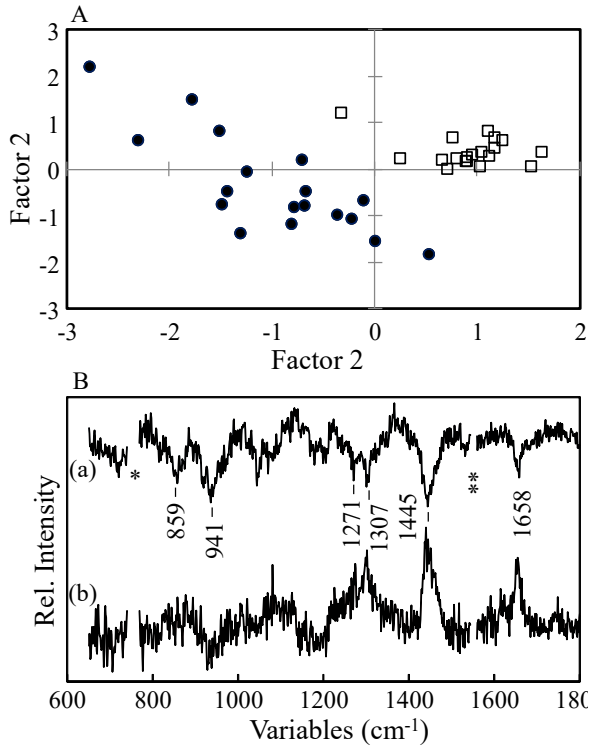

Fig. 2-7 Score and loading plots of the PLSR-DA model built for tumors (□; n = 10) and non-tumors (●; n = 18) tissues in a control (without any treatment) mouse. A score plot (A) for factor 1 and 2 and loading plots (B) of factor 1 (a), factor 2 (b), and factor 3 (c). (*: sapphire ball lens, **: oxygen)

Raman spectra were collected for non-tumor tissues in the colon of the colorectal

cancer mice models. The PLSR-DA method was applied to discriminate between tumor and non-tumor tissues. A score plot for factors 1 and 2 is depicted in Fig. 7A. The correlation coefficients were 0.997 and 0.781 for the calibration and validation for the discrimination model built with 3 factors. It demonstrates that endoscopic Raman spectroscopy is able to distinguish cancer tissue *in situ*. Loading plots for the factors 1 and 2 in Fig. 2-7B show characteristic features. In our previous study, a reduction in collagen was observed as the cancer advanced in the AOM/DSS colorectal cancer mouse model. Negative bands at 859 and 941 cm^{-1} in the loading plot of factor 1 (a) are assignable to hydroxyproline in collagen[37]. It suggests a reduction of collagen in the tumor tissues, in good agreement with our previous study. Bands at 1271, 1307, 1445, and 1658 cm^{-1} in the loading plot of factor 2 (b) are due to triacylglycerol in fat tissue[32,33]. The dispersion for the dataset of non-tumor tissue is larger than that of the tumor tissue. The normal colon wall consists of mucosa, muscle, and fat layers, and the thickness of the mucosa is not homogenous. In contrast, a polyp is covered with a thick layer of tumor cells with mucosal origin[38]. Because the working distance of the BHRP was 58 μm, the variety in collagen and fat concentration reflects the layer structure of the non-tumor tissue.

The effects of the anticancer drugs were examined in the non-tumor tissues. Raman spectra of non-tumor tissues were compared with the control and drug treated mouse models. Raman spectra of normal and tumor tissues after 5-FU treatment were evaluated with the PLSR-DA model built with datasets for normal and tumor tissues without drug treatment. The results (not shown) indicated that both the normal and tumor datasets were not classified as they should be, suggesting that 5-FU treatment modified molecular compositions in such tissues. A score plot of 4 datasets for normal and tumor

tissues, with and without 5-FU treatment, is depicted in Fig. 2-8A. The 4 datasets are classified into 4 independent categories, indicating that 5-FU affects not only cancer tissue but also normal tissue. PCA score plots of datasets for CDDP (B) and docetaxel (C) treated samples are also compared in Fig. 2-8. The datasets with drug treatment of normal and cancer tissues are similarly categorized in these plots. Previous reports showed that the efficacies of CDDP and docetaxel treatments were generally lower than that of 5-FU treatment for colorectal cancers. The present results suggest that Raman analysis is able to detect infiltration of anticancer drugs to the tissues but were not able to evaluate their efficacy. I did not suppose this result. It is neccesary to investigate these anticancer drug effects for normal colon tissues of mice without AOM/DSS treatment.

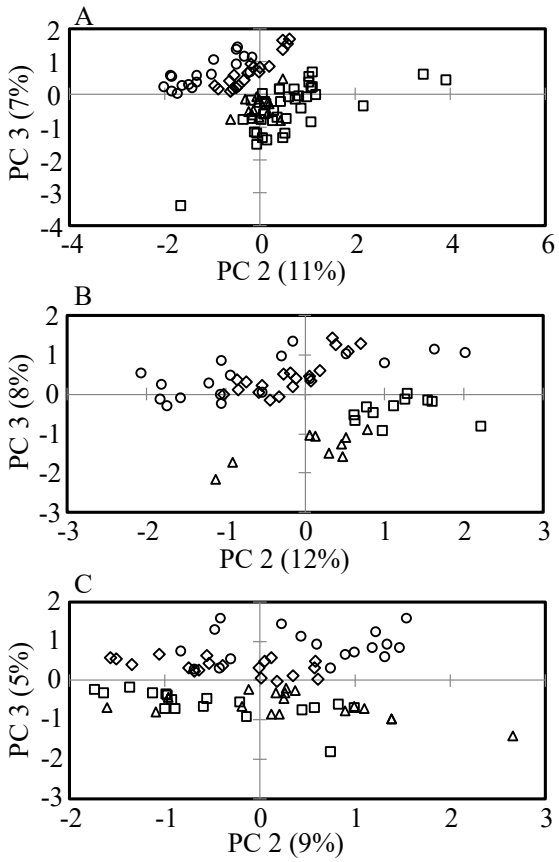

Fig. 2-8 Score plots of PCA models built with datasets of non-tumor and tumor tissues with and without drug treatments. Datasets of tumor lesions and non-tumor tissue of a control mouse are marked with ◇ and ○; those of tumor lesions and non-tumor tissue with drug treatment are marked with □ and △, respectively. Anticancer drugs are 5-FU (A), CDDP (B) and docetaxel (C)

Images of tumor tissues, measured Raman spectra and analysed in Fig. 2-6, stained with Masson's trichrome staining method are shown in Fig. 2-9. It colors stromal tissue that is generally rich in collagen I in blue and keratin in red.[39] The

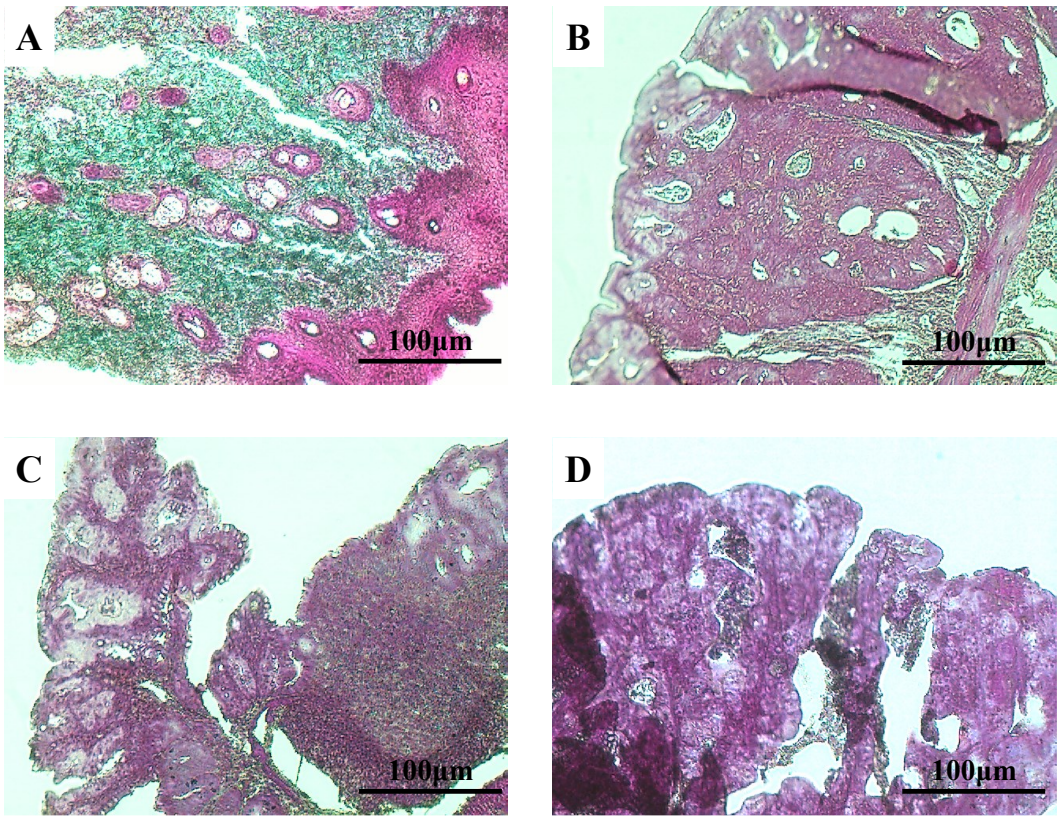

Fig. 2-9 Microscopic images of Masson's trichrome stained colorectal tumor tissues occurred in the lumen from the mucosal epithelium; treated with 5-FU (A), CDDP (B), docetaxel (C) and no treatment (D).

concentration of collagen reduces in advancing cancer, as observed in our previous study[23]. As such, I expected an increase in collagen in the anticancer drug-treated tissues. An image of cancer tissue treated with 5-FU (A) seems to have more green coloring compared with that of non-treated tissue (D). Images showing tissue treated with CDDP (B) and docetaxel (C) seem to have slightly higher blue components than non-treated tissue (D). This may indicate the efficacy of the anticancer drugs, but is difficult to come to any concrete conclusion. This pathological tissues was fixed with formaldehyde before analysis. It was not able to dye the lipid.

II - 5. Discussion

It is possible to study changes in the extracellular matrix and in cells using animal models, which cannot be achieved in experiments with cultured cells. In cancer tissues, it is especially important to observe variations in the density of collagen species. Although a doctor often prescribes multiple anticancer drugs for enhanced therapeutic benefit in real-life cancer therapy, reaction to a single drug is observed in the present study, making the results as simple to interpret as possible. Hence, the present animal study with mouse-sized Raman endoscopy is valuable. The results strongly indicate that Raman endoscopy was able to detect molecular changes induced by anticancer drugs in tumor tissue *in situ*.

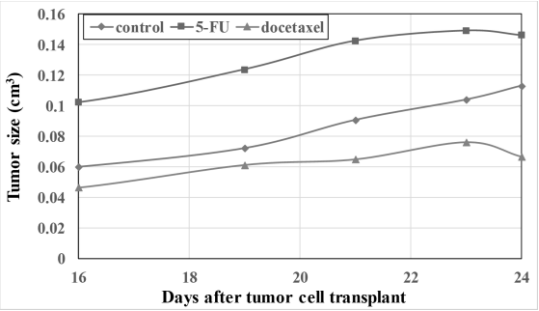

Fig.2-10 Tumor size in subcutaneous mouse models of DLD-1 (human colon adenocarcinoma cell line). Anticancer drugs, 5-FU and docetaxel, were administered at day 21.

The reduction of collagen species was observed in the cancer lesion, which was also observed in our previous study[23]. Although I expected increased collagen in the 5-FU treated cancer lesion, the molecular changes observed were instead attributed to changes in saccharides, DNA, RNA, and some amino acids. However, the endoscopic observations were performed after 2 weeks of drug treatment. This may be too early to expect to observe clear therapeutic effects in the tissue. In subcutaneous mouse models of DLD-1 (a human colon adenocarcinoma cell line), the tumor size was reduced 5 days after anticancer drug treatments with 5-FU and docetaxel (Fig. 2-10; no data for CDDP). Although those cancer cells are not the same as in the present spontaneous cancer model, it may be assumed that anticancer drugs will show efficacy in cancer tissues 2 weeks

following the initiation of therapy, at the molecular level at least. Although I refer to the surrounding tissue as “normal tissue,” it seems to be affected by inflammation induced by DSS administration. DSS causes diarrhea in the mouse model, which results in regeneration of endothelial cells. Since one of the mechanisms of 5-FU is interfering with DNA reproduction to induce apoptosis prior to cell division, 5-FU possibly induces inflammation in normal tissues as well as tumor cells.

The PLSR-DA results indicated that the 5-FU treated group had alterations in DNA, RNA, and amino acid composition. Because 5-FU is an analog of uracil as well as a disrupter of TS, it interferes with both DNA and RNA synthesis[13]. In contrast, the PLSR-DA suggested that the CDDP treated group had alterations in fat and protein species. CDDP builds cross-links between DNA strands in the double chain and blocks DNA duplication to induce apoptosis[14]. The results for the docetaxel treated tumors indicated increased fat concentration in the tissue. Docetaxel stabilizes tubulin to intercept the last stage of mitosis and induces apoptosis[15].

These 3 anticancer drugs, although having different mechanisms, showed characteristic spectral changes, suggesting that this technique is able to determine the type of cellular reaction induced in live cells within cancer lesions. The histopathological observation shows typical images of cancer tissue and stromal tissue was increased especially in 5-FU treatment. In contrast, the datasets of cancer tissues with and without drug treatment showed quite clear differences in the score plots and discrimination models. The spatial resolution of the present BHRP is estimated to be ~100 μm and the Raman spectrum represents the averaged molecular composition in the excitation volume, ~10^6 μm^3. The results of Raman data was not similar in MT staining in Fig.2-9. It is necessary to measure the deeper area by changing the material of the ball lens which is

much longer working distance in BHRP and to evaluate anticancer drug effects.

II - 6. Conclusion

Raman endoscopy has strong potential to detect effects of drug treatment in the digestive tract before the appearance of morphological changes. The Raman observation *in situ* showed a lower density of collagen species in cancer tissue, which is a good marker for discrimination of cancer lesions from normal tissue. Increased collagen should not be observed in the drug treated cancer lesions after 2 weeks of therapy. Molecular changes were observed but they were not specific to the cancer tissue. The discrimination model for cancer tissue is not valid to analyze the datasets of cancer and normal tissues with drug treatment, suggesting that the drug effects both normal and cancer tissues. It is difficult to determine drug efficacy from histopathological observation by the inexperienced observer. In contrast, Raman analysis is able to achieve this with BHRP and multivariate analysis, without any assessment by an experienced person. The present results demonstrate the potential of Raman endoscopy in the study of anticancer drug therapy. Raman analysis is highly sensitive to the effect of anticancer drugs. It is, however, necessary to conduct further detailed research to determine the therapeutic effect induced by anticancer drugs.

II - 7. References

1. Cancer statistics in Japan, *FPCR National Cancer Center*, 2015
2. A. Polk, K. Vistisen, M. Vaage-Nilsen and D. L. Nielsen, *BMC Pharmacology and Toxicology* 2014, **15**, 47
3. A. Polk, M. Vaage-Nilsen, K. Vistisen and D. L. Nielsen, *Cancer Treat. Rev.,* 2013, **8**, 974-984
4. W. E. Evans, M. V. Relling, *Science*, 1999, **286**, 487-491
5. M. S. Bergholt, W. Zheng, K. Lin, K. Y. Ho, M. The, K. G. Yeoh, J. B. Y. So and Z. Huang, *Analyst*, 2010, **135**, 3162–3168
6. D. W. Rosenberg, C. Giardina and T. Tanaka, *Carcinogenesis*, 2009, 30, 183–196
7. Y. Hattori, Y. Komachi, T. Asakura, T. Shimosegawa, G. Kanai, H. Tashiro and H. Sato, *Appl. Spectrosc*., 2007, **6**, 579–584
8. M. S. Bergholt, W. Zheng, K. Y. Ho, M. The, K. G. Yeoh, J. B. Y. So and Z. Huang, *J. Biomed. Opt*., 2011, **16**, 037003.
9. Y. Komachi, T. Katagiri, H. Sato and H. Tashiro, *Appl. Opt.,* 2009, **48**, 1683-1696
10. Y. Komachi, H. Sato, K. Aizawa and H. Tashiro, *Appl. Opt.,* 2005, **44**, 4722-4732
11. T. Katagiri, Y. S. Yamamoto, Y. Ozaki, Y. Matsuura and H. Sato, *Appl. Spectrosc*., 2009, **63**, 103-107
12. Y. S. Yamamoto, Y. Oshima, H. Shinzawa, T. Katagiri, Y. Matsuura, Y. Ozaki and H. Sato, *Anal. Chim.,* 2008, **619**, 8-13
13. C. N. Stemnberg, W. W. T. B. Huinink, J.F. Smyth, V. Bruntsch, L.Y. Dirix, N.A. Pavhdis, H. Franklin, S. Wanders, N. L. Bail and S.B. Kaye, *Br. J. Cancer,* 1994, **70**, 376-379
14. D. B. Longley,D. P. Harkin and P. G. Johnston, *Nat. Rev. Cancer,* 2003, **3**, 330-338

15. E. Grünberg, K. Ecrekt and H. R. Maurer, *Int. J. Oncol.* 1998, **12**, 957-963

16. H. K. Yosef, L. Mavarani, A. Maghnouj, S. Hahn, S. F. El-Mashtoly and K. Gerwert, *Anal. Bioanal. Chem.,* 2015, **407**, 8231-8331

17. S. Vinogradov, X. Wei, *Nanomedicine,* 2012, **7**, 597-615

18. S. Skolekova, M. Matuskova, M. Bohac, L. Toro, L. Demkova and J. Gursky, *Cell Commun. Signal.,* 2016, **14**,4

19. S. J. Grainger, J. V. Serna, S. Sunny, Y. Zhou, C. X. Deng and M. E. H. El-Sayed, *Mol. Pharm.* 2010, **7**, 2006-2019

20. J. Li, N. Hou, A. Faried, S. Tsutsumi, T. Takeuchi, and H. Kuwano, *Ann. Surg. Oncol.,* 2009, **16**, 761–771

21. Y. Tan, X. Sun, M. Xu, X. Tan, A. Sasson, B. Rashidi, Q. Han, X. Tan, X. Wang, Z. An, F. Sun, and R. M. Hoffman, *Clin. Cancer Res.*, 1999, **5**, 2157-2163

22. D. J. Dykes, M. C. Bissery, S. D. Harrison, Jr. and W. R. Waud, *Invest. New Drug,* 1995, **13**, 1-11

23. A. Taketani, R. Hariyani, M. Ishigaki, B. B. Andriana and H. Sato, *Analyst,* 2013, **138**, 4183-4190

24. C. Constantinides, R. Mean and B.J. Janssen, *ILAR e-journal,* 2011, **52**, e21-e31.

25. B. B. Andriana, Y. Oshima, S. Takanezawa, T. W. Tay, C. L. R. Soeratman, M. S. Alam, H. Mitsuoka, X. B. Zhu, T. Suzuki, Y. S. Yamamoto, N. Tsunekawa, Y. Kanai, M. Kurohmaru and H. Sato, *BiOS-SPIE, San Jose, California, USA,* 2009, 7167-33.

26. J. W. Chan, D. S. Taylor, T. Zwerdling, S. T. Lane, K. Ihara and T. Huser, *Biophys.J.,* 2006, **90**, 648–656

27. Y. Oshima, H. Shinzawa, T. Takenaka, C. Furihata and H. Sato, *J. Biomed. Opt.,* 2010, **15**, 017009.

28. Y. Oshima, H. Sato, A. Zaghloul, G. N. Foulks, M. C. Yappert and D. Borchman, *Curr. Eye Res.*, 2009, **34**, 824-835

29. T. H. Corbett, D. P. Griswold, B. J. Roberts, J. C. Peckham and F. M. Schabel, *Cancer,* 1977, **40**, 2660-2680

30. R. J. Lakshimi, V. B. Kartha, C. M. Krishna, J. G. R. Solomon, G. Ullas and P. U. Devi, *Radiat. Res.,* 2002, **157**, 175–182

31. N. Stone, C. Kendall, J. Smith, P. Crow and H. Barr, *Faraday Discuss.*, 2004, **126**, 141–157

32. C. Krafft, L. Neudert, T. Simat and R. Salzer, *Spectrochim.Acta, Part A*, 2005, **61**, 1529–1535

33. S. Fore, J. Chan, D. Taylor, T. Huser, *J. Opt.*, 2011, **13**, 044021.

34. I. Notingher, C. Green, C. Dyer. *J. R. Soc. Interface,* 2004, **1**, 79–90

35. R. Malini, K. Venkatakrishma, J. Kurien, K. M. Pai, L. Rao, V. B. Kartha and C. M. Krishna, *Biopolymers,* 2006, **81**, 179–193

36. L. Silveira, S. Sathaiah, R. A. Zangaro, M. T. Pacheco, M. C. Chavantes and C. A. Pasqualucci, *Laser Surg. Med.,* 2002. **30**, 290–297

37. H. U. Gremlich, B. Yan, *New York*, 2001, 421-476

38. M. D. Robertis, E. Massi, M. L. Poeta, S. Carotti, S. Morini, L. Cecchetelli, E. Signori, V. M. Fazio, *J. Carcinog.,* 2011, **10**, 9.

39. L. Cao, X. Qin, M. R. Peterson, S. E. Haller, K. A. Wilson, N. Hu, X. Lin, S. Nair, J. Ren, G. He, *J. Mol .Cell Cardiol.,* 2016, **92**, 185–195

Chapter III : Autofluorescence image and Raman spectroscopy for the *in situ* investigation of tumor constructions in live subcutaneous model mice

III - 1. Abstract

The site dependency in cancer tissue was evaluated using unstained autofluorescence hyperspectral imaging and Raman spectroscopy. The autofluorescence image reflected the distribution of the intact fluorescence materials such as nicotinamide adenine dinucleotide (NADH), flavin adenine dinucleotide (FAD), and collagen in the live subcutaneous tumor mouse model. Raman spectroscopy revealed the difference in blood flow between the active and non-active areas by NADH imaging. The autofluorescence image *in situ* and Raman image showed the distribution of type I collagen. The autofluorescence image *in situ* gathered information that was inaccessible from the tissue section of the sample. The combination of autofluorescence imaging and Raman spectroscopy may reflect the site dependency in cancer tissues.

III - 2. Introduction

The purpose of this study was to establish a noninvasive imaging technique for the *in situ* cancer diagnosis from cancer tissues. Histopathology, the gold standard for cancer diagnosis, allows decision-making based on visual observation. It is a type of pattern recognition procedure that discriminates between cancerous and normal tissues. The diagnosis of colorectal cancer is based on image observations, and mainly includes endoscopic observation, X-ray computed tomography (CT), magnetic resonance imaging (MRI), positron emission tomography (PET), and histopathology[1-5]. Images in Raman spectroscopy are obtained for the same purpose. The conventional imaging techniques allow visualization of tissue morphology but fail to reveal molecular information. In contrast, previous Raman studies suggest that the molecular composition of tissues is reflective of the development of cancer and the effects of anticancer agents[6,7]. Feofanov et al. reported confocal Raman microspectroscopy and imaging study of live cancer cells[8]. Zabaleta et al. reported imaging with surface-enhanced Raman scattering (SERS) nanotags in a live mouse[9]. Cancer tissue in general exhibits low uniformity and complex structures comprising differentiated tissue parts[10]. The excitation volume of general Raman instruments is quite small; for instance, it is 1 × 1 × 5 μm for a Raman microscope with a ×60 objective lens. As cancer tissue exhibits microstructure, its Raman spectrum may probably display site dependency. It may be difficult to collect information representing the whole lesion of the cancer tissue in a spot measurement. To acquire Raman images, a Raman microscope system with a raster scanning sample stage is commercially available. Raman images show molecular information without staining[11]. Many researchers are making efforts to develop an analytical method to extract molecular information from Raman images.

As Raman images are acquired Raman spectra from each point, the measurement may take several hours. It is necessary to use a sample fixed under a microscope. Raman image measurement is difficult to perform *in situ* using an endoscope. Other measurements are required to collect images of colorectal tumors *in situ* without surgery or staining. Autofluorescence has been studied for biomedical samples, especially for tissue analysis without staining or labeling. Autofluorescence is attributed to nicotinamide adenine dinucleotide (NADH) and flavin in viable cells and elastin and collagen from the extracellular matrices[12,13]. The maximum absorption and emission wavelengths for typical autofluorescence materials in tissues are well-studied[14-18]. Uedo et al reported the use of an autofluorescence image for the determination of colorectal tumors *in situ* with an endoscope[19].

During the acquisition of Raman spectral image by lateral scan, a spectrum is measured at each spot and the image comprises numerous measuring points, wherein each point has a total spectrum. Such an image consisting of spectra is referred to as a "hyperspectral image." Sato laboratory has a system that allows autofluorescence hyperspectral imaging (AF-HSI), and comprises an illumination part that emits monochromatic light in a tunable range from 250 to 800 nm, a detection part that produces an image in a tunable range from 400 to 1000 nm, and a hand-held probe connected to the detection part with an optical fiber. The AF-HSI system automatically collects images with different excitation and collection wavelengths. The detection part is equipped with band-pass filters and a highly sensitive charge-coupled device (CCD) camera. The full range of 250−800 nm excitation and 400−1000 nm detection may be measured in 600 s. Autofluorescence techniques have been applied for medical observations[20-22]. Diagnosis by autofluorescence and image measurement by Raman spectroscopy is studied. Kong et

al. reported that the basal cell carcinoma was discriminated *ex vivo* with 100% sensitivity and 92% specificity using autofluorescence and Raman imaging[23]. In contrast, the conventional Raman imaging system needs more than several hours to obtain Raman-HSI, owing to raster scanning. Reports suggest that SERS images were obtained from the living body with the delivery of nanoparticles into tissues[7,24]. With AF-HSI imaging, it is possible to obtain information on the tumor shape from the living body in a short period of time.

Here, the potential application of the AF-HSI system and Raman spectroscopy to evaluate colorectal tumors was investigated. The combination of AF-HSI images and Raman spectra was used at several points representing characteristic tissue types to study the relationship between fluorescence and Raman spectra at various microsites in the cancer tissue. The low uniformity of cancerous tissues may pose difficulty in comparison of the structure of cancer tissues in the absence of any information on the localization of the active cell division site. NADH and flavin adenine dinucleotide (FAD) are reportedly used to indicate cell viability. It is possible to identify the sites of active cell division in the cancer tissue by observing NADH. I examined the localization of NADH and collagen in the cancer tissue and decided to observe the composition differences by Raman spectroscopy. To evaluate AF-HSI, Raman images were obtained for the same tumor sample that was fixed and the results were compared with those of AF-HSI. A subcutaneous tumor mouse model was used for the study.

III - 3. Material and Methods

1. Preparation of DLD-1 subcutaneous cancer mouse model

BALB/c slc-*nu/nu* nude mice were purchased from SLC (Shizuoka, Japan).

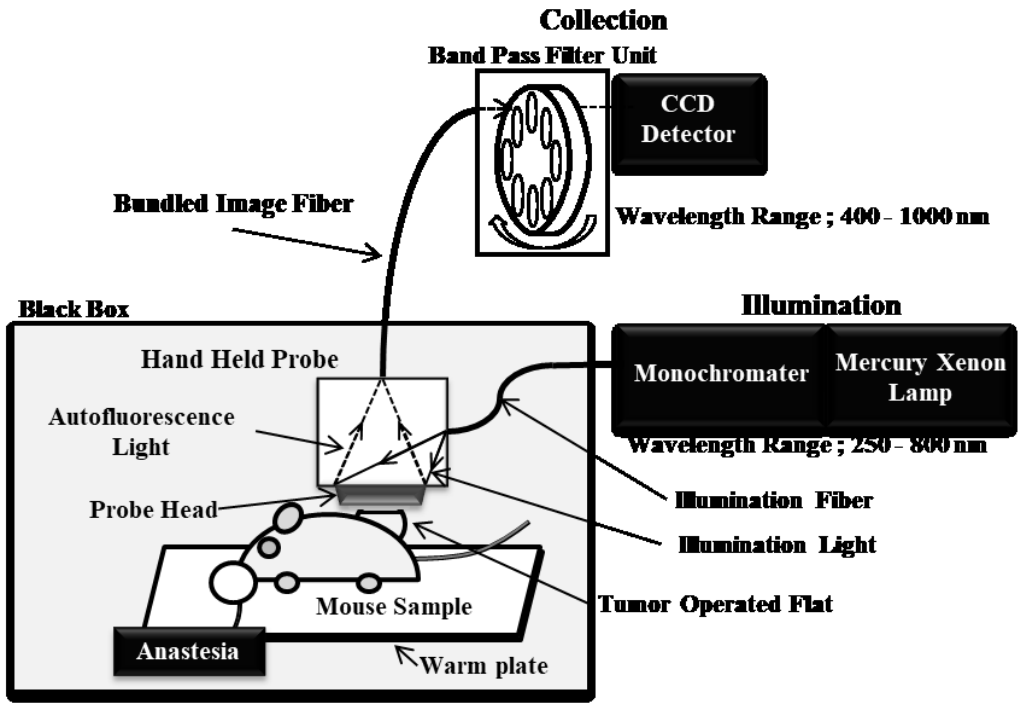

Fig.3-1 The structure of AF-HSI System. Illumination was 250-800 nm by monochromater and mercury xenon lamp. Collection was 400-1000 nm by band pass filter unit and CCD detector. Measuring sample was in block box to shut out lights from outside. Tumor was operated flat surgery.

DLD-1, a colorectal adenocarcinoma cell line, was implanted under the skin at the femur of 4-week-old mice at 1×10^6 cells/mL density in 0.1 mL normal saline. After 3 weeks, the tumor size was about 5 mm in diameter. The tumor was surgically exposed under anesthesia treatment by removing skin and cutting a part to observe the inside of the tissue. AF-HSI and Raman measurements were performed on the live tissue. The mouse was anesthetized using isoflurane (Wako Pure Chemical Industries, Ltd., Japan) and kept on a warming plate to maintain the body temperature to about 37°C. The animal procedure was approved by the ethics committee of Kwansei Gakuin University.

2. Autofluorescence hyperspectral imaging system

The schematic representation of AF-HSI system is provided in Fig. 3-1. The light

source was a mercury xenon lamp (500 W, L8288, Hamamatsu Photonics, Japan). The light was filtered and selected by a monochromator in a wavelength ranging from 250 to 800 nm by 10 nm of spectral resolution. The excitation light was transferred by an optical fiber to the hand-held probe. The collected by the prove was transferred into the detection unit by a bundled image filter light the image passed through a bandpass filter. The image of the specified wavelength was detected by a CCD (iXON DV887ECS-BV, Andor Technology Co. Ltd., Northern Ireland) with 512 × 512 pixels. The temperature of CCD was −68°C. The detection unit had 15 BP filters from 400 to 1000 nm with 40 nm step. The acquisition time was 1 s for each image. The measurement was performed by attaching the window of the probe head onto the sample. The measurable area of the probe was 5 × 5 mm.

3. Raman measurement

A Raman system equipped with BHRP was used for in situ Raman measurement in live mouse tumors. A diode laser (785 nm) was used for excitation. The laser power was 60 mW at the sample point. The Raman system used was the same mentioned in Chapter I and II. Raman spectra of subcutaneous tumors were collected at several points selected according to AF-HSI.

4. Raman imaging

The tumor tissue was fixed with 10% formaldehyde (Wako Pure Chemical Industries, Ltd., Osaka, Japan) for 24 h, dehydrated with ethanol, and subjected to paraffinization (Sakura Finetek, Tokyo, Japan). The paraffin-embedded tissue was sliced into 20-μm-thick pieces, and placed on a glass substrate. Paraffin was removed by xylene

and ethanol before measurement. Raman images were collected by Raman image system (inVia 417A48 Renishaw, UK). The laser wavelength was set at 532 nm and the exposure time was 10 s at each measured point. The sampling interval of the imaging was 100 μm, and the scanned area was 5000 μm × 5000 μm, including 2500 sampling points. HSI was analyzed by Wire software (Renishaw, UK).

5. Histopathological study

The resected whole tumor specimen was immediately fixed with 4% paraformaldehyde at 4°C, and dehydrated through a graded series of ethanol (70%, 80%, 90%, 95%, and 100%). The specimen was immersed in histo-clear and embedded in paraffin. Sections (5 μm thick) were prepared and stained with hematoxylin–eosin (H/E) or Masson's trichrome stain using HT15-1KT kit (Sigma-Aldrich Chemical Co., St. Louis, MO, USA) for histopathological study.

6. Data analysis

The image data obtained using AF-HSI were exported as a special file type, wherein the intensity measured at each excitation and detection wavelength was recorded as a binary value at each pixel. A homemade program made on Igor platform (WaveMetrics, US) was used to retrieve the image at a specific combination of wavelengths. A program was built to analyze the fluorescence image dataset that allowed the creation of a fluorescence image plot to be displayed in the image. Raman spectrum was treated repeatedly for five times to remove background noise using fifth polynomial line fitting. The spectral intensity was standardized with a phenylalanine band at 1003 cm^{-1}. Chemometrics software (Unscrambler; CAMO, USA) was used for principal

component analysis (PCA).

III - 4. Results

A subcutaneous tumor was grown in the femur of the mouse to a size of 0.06−0.12 cm^3. AF- and bright-field images of the tumor *in situ* are depicted in Fig. 3-2 (A-D), respectively. The image was obtained at 340 nm excitation and 460 nm collection wavelengths suitable for fluorescence. Image (B) was obtained with 450 nm excitation and 500 nm collection wavelengths suitable for FAD imaging. Image (C) was obtained using 450 nm excitation and 540 nm collection wavelengths suitable for collagen. NADH

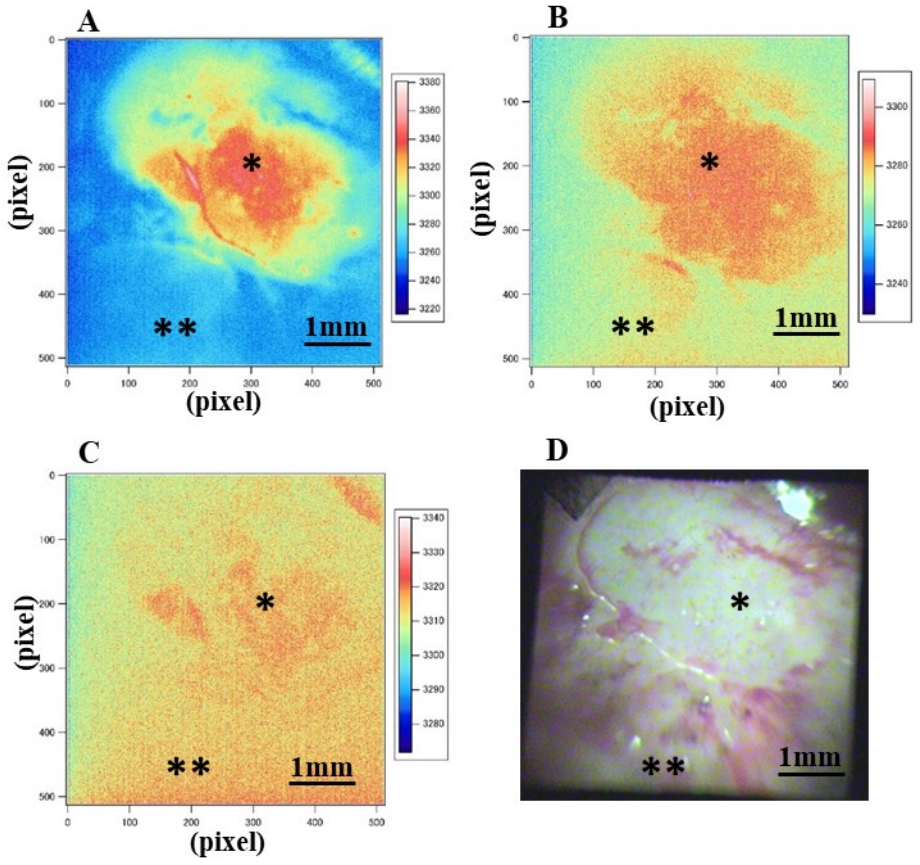

Fig. 3-2 AF- images of live tumor tissue and that of bright one. The topographies in A-C represent concentration of NADH (A), FAD (B) and collagen (C) respectively. The bright field image was collected at the same point where the AF-HSI was obtained.

and FAD exhibited almost the same localization in (A) and (B). Collagen had a larger area than NADH and FAD in (C). AF-HSI revealed the localization of NADH, FAD, and collagen in live cancer tissues. The distribution of autofluorescence from NADH (A) and collagen (C) was different within the same tumor. NADH is known as an indicator of cell viability, and collagen is a major component of the extracellular matrix. Fig. 3-2 (D) shows no difference between NADH active and non-active sites. AF-HSI provided a clear image reflective of the structure of the live tissue without any labeling.

Raman spectra of the tumor model are shown in Fig. 3-3. The spectrum (a) was obtained at an NADH active site that displayed strong signals, owing to NADH in the AF-HSI image in Fig. 3-2 (A). Cancer cells have higher NADH levels than normal cells, owing to their glycolysis[25]. It is assumed that the NADH active site is dominated by all proliferating cells, especially in the cancer tissue. Spectrum (b) was obtained at NADH non-active site. The spectrum obtained from the subtraction of (b) from (a) is depicted in Fig 3-3 (c). These bands are assigned to amide I (1654 cm^{-1}), CH deformation (1304 and 1440 cm^{-1}), amide III vibrational modes (1263 cm^{-1}) and a respiratory mode phenyl group (1003 cm^{-1})[26]. In the difference spectrum (c), a sharp peak was observed at 1435 cm^{-1} in the positive direction, attributable to

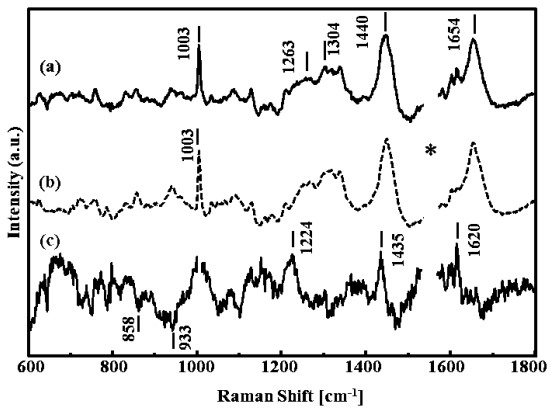

Fig. 3-3 Raman spectrum of NADH in the tumor model tissue shown active place and (b) is from NADH non-active place in fig.2. (c) is subtracted spectra of (a) – (b). (* is oxygen from BHRP) Characteristic bands due to proteins which are rich in tissue are observed at 1654, 1440, 1304, 1263 and 1003 cm^{-1}.

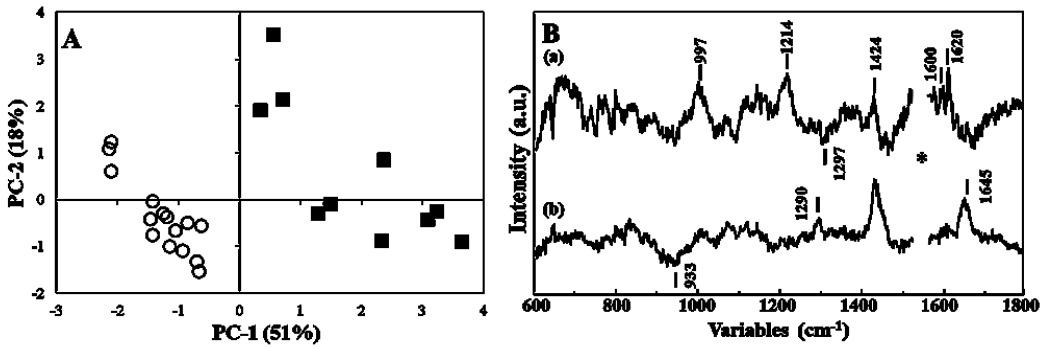

Fig.3-4 (A) is score plot of principal component analysis of Raman spectra obtained from DLD-1 tumor. ■ is from the part (a), ○ is the spectrum from the part (b) in Fig.3. (B) is loading plot of principal component analysis of Raman spectra obtained from DLD-1 tumor. (a) shows PC1, and (b) shows PC2. (* is oxygen from BHRP)

the CH_3 deformation mode of alkyl chains of lipid with relatively long chains[27]. Bands corresponding to the heme group in hemoglobin were observed at 1620 cm^{-1} [28]. Negative bands at 858 and 933 cm^{-1} corresponded to collagen. Subtracted spectra of active and non-active site showed differences in lipid, blood, and collagen concentrations. Raman spectra of NADH active and non-active sites were clearly different. It was difficult to observe the structure of the tissue without any staining under the bright field.

Fig. 3-4 depicts the PCA score plot (A) and loading plots of PCs. PCA was applied to the datasets of NADH active and non-active sites. The contribution of PC1 was 51%, much higher than that of PC-2 (18%). PC-1 loading was almost the same as that observed from the subtraction spectra of Fig. 3-3 (c). The dataset of NADH active sites was well discriminated from that of NADH non-active sites, especially by PC1. In the loading plot of PC1, a strong band appeared in the positive direction at 997 cm^{-1} and was attributable to the CO single bond in monosaccharides[29]. The band at about 1122 cm^{-1} corresponded to C-O-C symmetric oscillation of polysaccharides[30]. The band associated with deoxyribose was observed at 1424 cm^{-1} in the positive direction[31]. Bands at 1214,

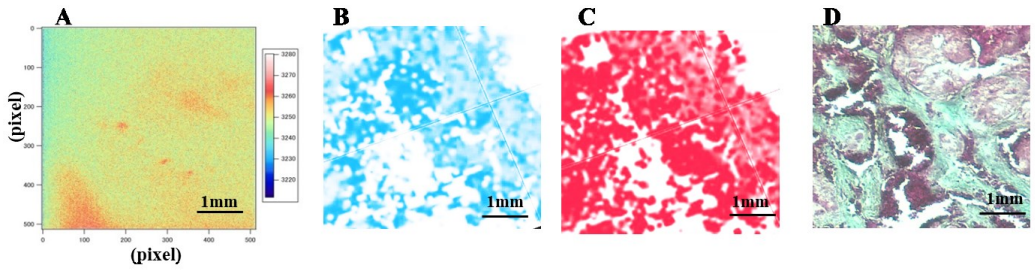

Fig. 3-5 (A) is AF- image of collagen I. (B) is collagen Raman image using 858 cm^{-1} Raman band intensity. (C) is protein Raman image using 1654 cm^{-1} Raman band intensity. (D) is Masson's trichrome staining of same place.

1600, and 1620 cm^{-1} were probably related to the heme group in hemoglobin. PCA results showed that NADH active sites in the tumor were richer in saccharides, deoxyribose, and hemoglobin than the non-active sites.

The AF image (A) reflected collagen I measured at 450 nm excitation and 540 nm detection wavelengths in Fig. 3-5. Raman images of the resected cancer tissue were compared to AF-HSI images. The Raman image of (B) reflected the intensity of Raman band at 858 cm^{-1} for collagen I, whereas the image of (C) was associated with the intensity of a band at 1654 cm^{-1} for proteins. The collagen I distribution in these images was different. Masson's trichrome staining in (D) showed collagen-like stromal tissues that stained blue. These tissues were rich in collagen. HE and Masson's trichrome staining

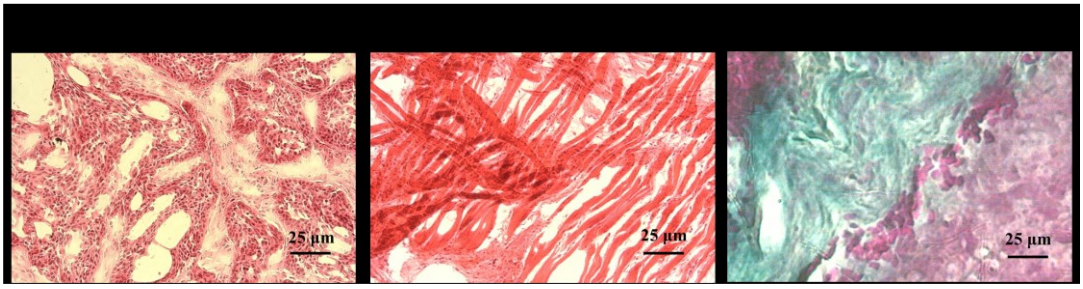

Fig. 3-6 A and B are picture of HE staining of DLD-1 tumor. C is picture of Masson's trichrome staining of DLD-1 tumor. A is observed a part where cells are densely collected or a part where fibrosis is progressed. B is the state of the connective tissue can be observed. C is observed stromal tissue that was stained blue.

images of the tumor tissue observed with Raman imaging and AF-HSI in Fig. 3-5 are depicted in Fig. 3-6. In (A), cells are densely packed in a space surrounded by fibrosis. In (B), the tissue is dominated by connective tissues and very few cells could be seen. In Masson's trichrome-stained image (C), the stromal tissue was stained blue, indicating that the stromal tissue was rich in collagen. HE-stained images of tumors showed varied distribution patterns within the same tumor (Fig. 3-6). As both NADH and FAD have a similar coenzyme for oxidoreductase, the AF-HSI image of NADH was similar to that of FAD.

III - 5. Discussion

The results of PCA described in Fig. 3-4 suggest that AF-HSI and Raman spectroscopy have the potential to identify the region involved in cancer cell division. It has been confirmed that NADH active sites exhibited more saccharides, deoxyribose, and hemoglobin than non-active sites. Cancer tissues consume a large amount of glucose to facilitate repetitive cell division through angiogenesis[10,25]. From these facts, NADH active site was thought to be the region involved in the angiogenesis and cell division. NADH Raman band appeared at 1546, 1557, 1620, and 1676 cm^{-1} [32,33]. However, these results showed a few typical NADH bands, given that Raman spectroscopy collects several types of molecules, proteins, lipids, and blood other than NADH. AF-HSI was a good guide to distinguish between NADH active and non-active sites in the live tissue to perform studies with Raman spectroscopy.

Both AF-HSI and Raman images described in Fig. 3-5 reveal the difference in the localization of collagen I. As the AF-HSI image was acquired from the living body, the autofluorescence information was acquired from deeper tissues as against the data

obtained from the 20-μm tissue section in Raman images. The comparison between the Raman images for collagen I and proteins indicate the relatively correct localization of collagen I in Raman images. A Raman band of 858 cm^{-1} was used for imaging, as this band was a better representative of collagen I than the band at 933 cm^{-1}. A Raman image of proteins using 1654 cm^{-1} showed localization of all proteins, including collagen. However, images with a single band have low confidence. It is necessary to prepare a program to describe more confirmed images using multiple bands.

III - 6. Conclusion

In this study, AF-HSI images were successfully obtained for live tumor tissues. Raman analysis revealed higher blood flow rate in the NADH active site than in the non-active site in tumors. The distributions of collagen observed by Raman imaging was different from that detected using AF-HSI. AF-HSI images with a single excitation and detection wavelength were acquired in a second. This study demonstrates the potential of the HSI system and AF-HSI in the study of colorectal tumors to enable structure differentiation in cancer tissues. The combination of autofluorescence imaging and Raman spectroscopy has potential applications for *in situ* cancer diagnosis.

III - 7. Reference

1. P. Hewitson, P. Glasziou, E. Watson, B. Towler and L. Irwig, *Am. J. Gastroenterol.,* 2008, **103**, 1541-1549
2. K. W. Kinzler and B. Vogelstein, *Cell,* 1996, **87**, 159-170
3. O. A. Ogunbiyi, F. L. Flanagan, F. Dehdashti, B. A. Siegel, D. D. Trask, E. H. Birnbaum, J. W. Fleshman, T. E. Read, G. W. Philpott and I. J. Kodner, *Ann. Surg. Oncol.*, 1997, **4**, 613-620
4. T. Ichikawa, S. M. Erturk, U. Motosugi, H. Sou, H. Iino, T. Araki and H. Fujii, *AJR*, 2006, **187**, 181-184
5. D. Dominique, *J. Nucl. Med.,* 1999, **40**, 591-603
6. A. Taketani, R. Hariyani, M. Ishigaki, B. B. Andriana and H. Sato, *Analyst*, 2013, **138**, 4183-4190
7. A. Taketani, B. B. Andriana, H. Matsuyoshi and H. Sato, *Analyst*, 2017, **142**, 3680–3688
8. A. V. Feofanov, A. I. Grichine, L. A. Shitova, T. A. Karmakova, R. I. Yakubovskaya, M. E. Charlier and P. Vigny, *Biophys. J.,* 2000, **78**, 499–512
9. C. L. Zavaleta, B. R. Smith, I. Walton, W. Doering, G. Davis, B. Shojaei, M. J. Natan and S. S. Gambhira, *PNAS*, 2009, **106**, 13511–13516
10. D. Hanahan and R. A. Weinberg, *Cell*, 2000, **100**, 57-70
11. S. Keren, C. Zavaleta, Z. Cheng, A. de la Zerda, O. Gheysens, and S. S. Gambhir, *PNAS*, 2008, **105**, 5844–5849
12. J. E. Aubin, J. *Histochem. Cytochem.,* 1979, **27**, 36-43
13. G. M. Barenboim, A. N. Domanskii, K. K. Turoverov, *New York*, 1969
14. K. T. Schomacker, J. K. Frisoli, C. C. Compton, T. J. Flotte, J. M. Richter, N. S.

Nishioka, *Lasers Surg. Med.,* 1992, **12**, 63-78

15. B. Palcic, S. Lam, J. Hung, C. MacAulay, *CHEST,* 1991, **99**, 742-743
16. S. Takehana, M. Kaneko, H. Mizuno, *Diagn. Ther, Endosc.,* 1999, **5**, 59-63
17. S. Lam, T. Kennedy, M. Unger, Y. E. Miller, D. Gelmont, V. Rusch, B. Gipe, D. Howard, J. C. LeRiche, A. Coldman, *CHEST,* 1998, **113**, 696-702
18. T. Ogihara, H. Watanabe, A. Namihisa, O. Kobayashi, H. Miwa, N. Sato, *Diagn*. *Ther. Endosc.*, 1999, **5**, 119-124
19. N. Uedo, H. Iishi, M. Tatsuta, T. Yamada, H. Ogiyama, K. Imanaka, N. Sugimoto, K. Higashino, R. Ishihara, H. Narahara and S. Ishiguro, *Gastroint. Endosc.*, 2005, **62,** 521-528
20. N. Uedo, K. Higashino, R. Ishihara, Y. Takeuchi and H. Iishi, *Dig. Endosc.*, 2007, **19**, 134–138
21. Y. J. Sepah, A. Akhtar, M. A. Sadiq, Y. Hafeez, H. Nasir, B. Perez, N. Mawji, D. J. Dean, D. Ferraz and Q. D. Nguyen, *Saudi J. Ophthalmol.,* 2014, **28**, 111–116
22. K. Ottolino-Perry, E. Chamma, K. M .Blackmore, L. Lindvere-Teene, D. Starr, K. Tapang, C. F. Rosen, B. Pitcher, T. Panzarella, R. Linden and R. S. DaCosta, *Int. Wound J.,* 2017, **14**, 833-841
23. K. Kong, C. J. Rowlands, S. Varma, W. Perkins, L. H. Leach, A. A. Koloydenko, H. C. Williams and L. Notingher, *PNAS*, 2013, **110**, 15189-15194
24. S. Harmsen, R. Huang, M. A. Wall, H. Karabeber, J.M. Samii, M. Spaiiviero, J. R. White, S. Monette, R. O'Connor, K. L. Pitter, S. A. Sastra, M. Saborowski, E. C. Holland, S. Singer, K. P. Olive, S. W. Lowe, R. G. Blasberg and M. F. Kircher, Sci. Transl. Med., 2016, **7**, 271-293
25. J. Fan, T. Hitosugi, T. W. Chung, J. Xie, Q. Ge, T. L. Gu, R. D. Polakiewicz, G. Z.

Chen, T. J. Boggon, S. Lonial, F. R. Khuri, S. Kang and J. Chen, *Mol. Cell. Biol.,* 2011, 31, 4938-4950

26. J. W. Chan, D. S. Taylor, T. Zwerdling, S. M. Lane, K. Ihara, T. Huser, *Biophys. J.*, 2006, **90**, 648-656
27. C. Krafft, L. Neudert, T. Simat, R. Salzer, *Mol. Biomol. Spectrosc.,* 2005, **61**, 1529-1535
28. H. Sato, H. Chiba, H. Tashiro, Y. Ozaki, *J. Biomed. Opt.,* 2001 **6**, 366-370
29. R. K. Dukor, Vibrational spectroscopy in the detection of cancer. *Handbook of Vibrational Spectroscopy*, 2001
30. G. Shetty, C. Kendall, N. Shepherd, N. Stone, H. Barr, *Br. J. Cancer,* 2006, **94**, 1460-1464
31. A. J. Ruiz‐Chica, M. A. Medina, F. Sanchez‐Jimenez, F. J. Ramirez, *J. Raman Spectrosc.,* 2004, **35**, 93-100
32. K. T. Yue, C. L. Martin, D. Chen, P. Nelson, D. L. Sloan and R. Callender, *Biochem*., 1986, **25**, 4941-4947
33. Z. Movasaghi , S. Rehman and I. U. Rehman, *App. Spectrosc. Rev.*, 2007, **42**, 493–541

General Conclusion

Improvement in the accuracy of endoscopic technology is desirable for the accurate diagnosis of colorectal cancer. Here, Raman spectroscopy was used to support endoscopic diagnosis in a mouse model. The first study demonstrates that the mRE system and BHRP were able to measure colorectal tumors in the mouse model *in situ*. The advancement in colorectal tumor growth was simultaneously monitored to obtain spectral changes and visual information about the decrease in collagen I in the same tumor of a live mouse over several weeks of observation. In this study, I observed shrinking tumor and I collected Raman spectra from this tumor continuously. LDA results judged that this shrinking tumor was still colorectal tumor. The mRE system has potential applications in cancer diagnosis without morphological discrimination and Raman spectroscopy may serve as a supporting technique to improve the accuracy of endoscopic diagnosis. The second study demonstrates the potential of the mRE system with BHRP in the study of the effects of anticancer drugs. The effects of anticancer drugs on colorectal tumors were monitored using the mRE system. The mRE system is a powerful instrument that allowed monitoring of changes in the tumor morphology following drug treatment. Raman spectroscopy may be used to confirm the therapeutic effects of drugs and determine the left-over cancer tissue, if any, after tumor treatment. In addition, the mRE system and mouse model may be used to evaluate the effects of the drug through direct observation of colorectal tumors *in situ*. The third study demonstrates the collection of autofluorescence images from cancer tumors *in situ* and its application for the detection of active points in tumors. Raman spectroscopy showed the site dependency of colorectal tumors. Although the result revealed the relationship between the AF-HSI and Raman images, confirmatory studies are needed. AF-HSI images may be useful to observe the

site dependency of colorectal tumors.

The measurement method using a mouse model, Raman spectroscopy, and AF-HSI imaging may serve as an important tool in fundamental research to study cancer progression and effects of anticancer drugs. It is possible to create an analytical model based on the progression of cancer, and Raman spectroscopy may be established as a supporting technology for the endoscopic diagnosis of cancers.

Acknowledgements

In this research, I deeply appreciate Professor Hidetoshi Sato who received guidance from Faculty to Doctoral Course for the 8th grade gently and gratefully, and I would like to express my deepest gratitude to the faculty members of Department of Life Sciences major. Also, I would like to express my deepest gratitude to Bibin. B. Andriana Assistant Professor, Assistant Professor Hiroko Matsuyoshi, Dr. Mika Ishigaki, Dr. Yasuhiro Maeda and members of Sato Laboratory.

Finally, I am grateful to my parents for supporting graduate school life.

List of Publications

List of papers

First Author

1. Akinori Taketani, Retno Hariyani, Mika Ishigaki, Bibin B. Andriana and Hidetoshi Sato, "Raman Endoscopy for the *in situ* investigation of advancing colorectal tumors in live model mice" *Analyst*, 2013, **138**, 4183-4190

2. Akinori Taketani, Bibin B. Andriana, Hiroko Matsuyoshi and Hidetoshi Sato, "Raman Endoscopy for Monitoring Anticancer Drug Treatment of Colorectal Tumors in Live Mice" *Analyst*, 2017, **142,** 3680–3688

Co-Author

1. Mika Ishigaki, Yasuhiro Maeda, Akinori Taketani, Bibin B. Andriana, Ryu Ishihara, Kanet Wongravee, Yukihiro Ozaki and Hidetoshi Sato, "Diagnosis of early-stage esophageal cancer by Raman spectroscopy and chemometric techniques." *Analyst*, 2016, **141**, 1027-1033